Effect of Laser Welding Parameters on 6061 Aluminium Alloy

D.Narsimhachary

(611MM301)

DEPARTMENT OF METALLURGICAL AND MATERIALS ENGINEERING

NATIONAL INSTITUTE OF TECHNOLOGY ROURKELA

ODISHA-769008.

2014

Effect of Laser Welding Parameters on 6061 Aluminium Alloy

Thesis submitted to the National Institute of Technology Rourkela

For the award of the degree of

M.Tech [Research]

By

D.Narsimhachary

(611MM301)

DEPARTMENT OF METALLURGICAL AND MATERIALS ENGINEERING

NATIONAL INSTITUTE OF TECHNOLOGY ROURKELA

ODISHA-769008.

2014

Effect of Laser Welding Parameters on 6061 Aluminium Alloy

Thesis submitted to the National Institute of Technology Rourkela

For the award of the degree of

M.Tech [Research]

By

D.Narsimhachary

(611MM301)

Under the supervision of

Prof. Anindya Basu

DEPARTMENT OF METALLURGICAL AND MATERIALS ENGINEERING

NATIONAL INSTITUTE OF TECHNOLOGY ROURKELA

ODISHA-769008.

2014

I Dedicate This Thesis to my DAD

DEPARTMENT OF METALLURGICAL AND MATERIALS ENGINEERING

NATIONAL INSTITUTE OF TECHNOLOGY, ROURKELA, ODISSA, 769008

CERTIFICATE

This is to certify that the thesis entitled "**Effect of Laser Welding Parameters on 6061 Aluminium Alloy**" being submitted by Mr. **D.NARSIMHACHARY** to the National Institute of Technology, Rourkela, for the award of the degree of **Masters of Technology (Research)** is a record of bonafide research work carried out under my supervision and guidance. The results presented in this thesis have not been submitted elsewhere for the award of any other degree or diploma.

This work in my opinion has reached the standard of fulfilling the requirements for the award of the degree of **Masters of Technology (Research)** in accordance with the regulations of institute.

Date: ----------

Prof: Anindya Basu

(Supervisor)

AKNOWLEDGMENT

The happiness and excitement that accompany the successful completion of a task would be incomplete without the mention of the people who made it possible and whose endless guidance and encouragement crowned all the efforts with success.

Therefore, I would like to take this chance to express my sincere and heartfelt gratitude to all those who made this report possible.

At first I would like to thank My Guide, Thesis supervisor **Prof Anindya Basu,** Department of Metallurgical & Materials Engineering, National Institute of Technology, Rourkela who not only permitted me to work at International Advanced Research Centre for Powder Metallurgy & New Materials (ARCI) Hyderabad, but also helped me as friend without his guidance, untiring efforts and meticulous attention at all stages during research work I could not complete my work.

I express my sincere gratitude to **Dr. G .Padmanabham**, Team leader, Centre for laser processing of material (CLPM), Associate Director ARCI, for his kind gesture for permitting me to carry out the Laser welding work at Centre for Laser Processing of Material (CLPM) ARCI Hyderabad. He was a great motivator and enlightened me with his valuable suggestions. With his constant encouragement and able guidance during every stage of the experimental work the research work came to a successful completion

I wholeheartedly thank **Dr. Ravi Nathuram Bathe**, Scientist of ARCI, Hyderabad, for his constant support, encouragement and guidance during every stage of the experimental work that brought this work to a successful completion.

I thank **Prof. B.C.Ray** Head of the Department, Department of Metallurgical and Materials Engineering, National Institute of Technology, Rourkela, for permitting me to carry out this work at ARCI.

I also gratefully acknowledge the support of **Dr. Nithin Wasaker**, Scientist, ARCI, for helping me in carrying out fatigue experiments and **Dr.N.Ravi** Scientist, ARCI, for Tensile Testing during the period.

I would like to thank **Prof J. Dutta Mazumdar,** Department of Metallurgical and Materials Engineering, IIT, Khargpur, for permitting me to carry out the corrosion experiments in her laboratory.

I would like to convey my gratitude to **Prof. Debdulal Dash,** Department of Metallurgy and Materials Engineering, Bengal Engineering and Science University, Howrah for allowing me carry out the formability test.

I am also thankful to **Mr. S. Pradhan**, Department of Metallurgical and Material Engineering, NIT, Rourkela for his help during the execution of SEM.

I am also thankful to **Mr. Arindam Pal**, Department of Metallurgical and Material Engineering, NIT, Rourkela for his help to carry out the XRD analysis.

I would like to thank all my **Friends** for making my stay colorful and without their help I couldn't have reached this stage.

All along this work my **parents** and all other **family members** were my greatest sources of inspiration, strength and assurance. I take this opportunity to acknowledge the sacrifices made by them towards my upbringing and who patiently endured my absence for long time; their constant encouragement helped me to move ahead with the program

(D. Narsimhachary)

611MM301

Metallurgical & Materials Engineering

NIT Rourkela, Odisha.

CONTENTS

Certificate

Acknowledgments

Contents

List of Figures i

List of Tables iv

Abstract v

Chapter 1. Introduction **1**

1.1 Background 1

1.2 Motivation 2

1.3 Problem Definition 3

1.4 Outline of the Thesis 3

Chapter 2. Literature Review **4**

2.1 Introduction to Laser 4

2.1.1 Generation of Laser 5

2.2 Laser Welding 7

2.3 Aluminium alloys 11

2.4 Weldability of Aluminium alloys 14

2.5 Laser Welding of Aluminium and Aluminium alloys 15

Chapter 3. Experimental Work **18**

3.1 Introduction 18

3.2 Base Material 18

3.3 Sample Preparation 18

3.4 Welding Experiments 19

3.4.1 Screening Experiments 21

3.4.2 Butt Welding Experiments 21

3.5 Post Welding Experiments 22

3.6 Characterisation of Welds 22

3.6.1 XRD Analysis 22

3.6.2 Macro and Microstructural Examination 23
3.6.3 Mechanical Characterization 23
3.7 Corrosion Test 25

Chapter 4. Effect of Laser Welding Parameter on Single Bead Welds 27
4.1 Introduction 27
4.2 Effect of Welding Parameters in BOP Experiments 27
4.3 Laser Butt Welding 33
4.3.1 XRD Analysis 33
4.3.2 Macro and Microstructural Analysis 34
4.3.3 Hardness Study 37
4.3.4 Tensile Testing 39
4.3.5 Fractography 40
4.3.6 Formability Study 41
4.3.7 Weld Thermal Profile Analysis 44
4.4 Summary 45

Chapter 5. Effect of Laser Welding Parameter for Bead over Bead Welds 46
5.1 Introduction 46
5.2 Effect of Welding Parameters in BOP Experiments 46
5.3 Bead over Bead Laser Butt welding (Double pass) 47
5.3.1 Macrostructures 48
5.3.2 XRD Analysis 49
5.3.3 Microstructures 49
5.3.4 Micro Hardness Study 50
5.3.5 Tensile Testing 51
5.3.6 Fractography 52
5.3.7 Formability Study 52
5.3.8 Fatigue Testing 53
5.3.9 Corrosion Test 55
5.4 Summary 56

Chapter 6. Conclusion 58

Reference 59

Bio Data 64

LIST OF FIGURES

Fig. 2.1: Schematic Setup of Laser 6

Fig. 2.2: Schematic set up of solid state Nd-YAG Laser with optical fiber Transmission system 7

Fig. 2.3: Schematic Representation of laser welding. 8

Fig. 2.4: (a) Conduction melt pool (semi-circular) (b) deep-penetration (key hole) Welding 11

Fig. 3.1: Experimental plan 19

Fig. 3.2: Schematic of CO_2 slab laser. 20

Fig. 3.3: Tensile specimen dimensions 24

Fig. 3.4: Fatigue specimen dimension 24

Fig. 3.5: Die and Punch design used in Erichsen formability test 25

Fig. 3.6: Schematic of corrosion test setup 26

Fig. 4.1: Effect of Laser parameters and shielding gas flow-rates on penetration 29

Fig. 4.2: EDS line scan from base material to base material on weld obtained with 3 kW power, 3 m/min welding speed, 18 l/min flow rate helium shielding gas 29

Fig. 4.3: Coupling behavior: (a) No Coupling and (b) Coupled 30

Fig. 4.4: Effect of welding speed on coupling behavior 30

Fig. 4.5: Coupling behavior with (a) Argon and (b) Helium 31

Fig. 4.6: Effect of shielding gas on the depth of penetration and throat width, (a) With Argon, (b) with Helium and (c) without shielding gas. 32

Fig. 4.7: XRD plot of (a) base material, b) as welded condition (He-18 l/min, 3 kW Power, 4 m/min speed, Ar-22 l/min, 3 kW Power, 3.5 m/min

Speed, without shielding-3 kW Power, 4.5 m/min speed) and (c) after post Welding heat treatment of weld made with He (170^{o}C for 6hrs) 33
Fig. 4.8: Butt welds with varying shielding gas conditions 34
Fig. 4.9: Optical micrograph of Base Material (AA 6061 alloy) 35
Fig. 4.10: Microstructures of welds with different shielding conditions 35
Fig. 4.11: SEM photograph of fusion line of the weldments 36
Fig. 4.12: SEM photograph of FZ of the weldments 37
Fig. 4.13: Microhardness profile on cross sectional surface of laser welded aluminium alloy in (a) as welded and (b) after post welding heat treated Conditions (with Helium as shielding gas) 38
Fig. 4.14: Elemental Mapping of FZ of weld with no shielding condition 40
Fig. 4.15: Fractured surface of (a) base material; welded with (b) Helium (c) Argon (d) No-Gas. 41
Fig. 4.16: Erichsen Index (I.E.) of base material and welded samples obtained By Erichsen Cupping test. 41
Fig. 4.17: Appearance of (a) Base material and (b) Single pass weld after Erichsen Cupping test. 42
Fig. 4.18: Temperature distribution at different locations 43
Fig. 4.19: Temperate distribution from Centre line 43
Fig. 4.20: Effect of cooling rate 44
Fig. 5.1: Macrostructures of BOP welds 47
Fig. 5.2: Macrostructure of (a) single pass and (b) double pass 48
Fig. 5.3: Effect of welding condition on throat width and depth of penetration 49
Fig. 5.4: XRD plot of Double Pass Weld (3 kW Power, 4 m/min speed, Donut mode + 2.5 kW Power, 6 m/min speed, Gaussian mode) 49

Fig. 5.5: Microstructures of (a) single pass FZ, and (b) Double pass FZ, (c) single pass fusion line and (d) double pass fusion line. 50
Fig. 5.6: Hardness profile of single pass and double pass welds (He gas) 51
Fig. 5.7: Fractured surface of (a) single and (b) double pass welds. 52
Fig. 5.8: Erichsen Index (I.E.) of single and double pass welded samples obtained by Erichsen Cupping test. 53
Fig. 5.9: Appearance of (a) Single pass weld (b) Double pass weld after Erichsen Cupping test. 53
Fig. 5.10: Fatigue result of base material, single pass and double pass welds. 54
Fig. 5.11: Potentio-dynamic polarization behavior of base material, single pass and Double pass welds. 55
Fig. 5.12: Post corrosion SEM micrograph of (a) base material (b) single pass and (c) Double pass weld. 56

LIST OF TABLES

Table 3.1: Chemical composition of AA6061 alloy (wt. %) 18

Table 3.2: Parameters for Bead on Plate welding 21

Table 3.3: Parameters for Butt Welding 22

Table 4.1: Parameters for butt welds 33

Table 4.2: EDS analysis based on Fig. 4.11 36

Table 4.3: EDS analysis based on Fig.4.12 37

Table 4.4: Tensile results of Base material and single pass welds with Varying shielding gas condition at He-18l/min, 3 kW Power, 4 m/min Speed, Ar-22 l/min, 3 kW Power, 3.5 m/min Speed, Without shielding-3 kW Power, 4.5 m/min Speed, Post weld Treatment (170^{o}C for 6 hrs). 39

Table 5.1: BOB Butt welding parameters. 48

Table.5.2: Tensile results of single pass and double pass welds (He gas) 51

Table 5.3: Summery of potentio-dynamic test result 55

ABSTRACT

Aluminium alloys are widely used in aircraft industry which involves a large number of joint configurations, traditionally fabricated by riveting. Disadvantages of riveting are extra weight to the structure, stress concentration, crevices corrosion and loosening due to vibrations. Moreover, it is a time consuming and manpower intense task. Laser welding can be a potential tool which is superior to other joining techniques, such as, arc welding due its heat input nature and related microstructural effect.

The present study is focused on improving metallurgical and mechanical characteristics of aluminium alloy (6061-T6) sheet butt welds obtained by common single pass CO_2 laser by refining the microstructure with extra laser pass/remelting. Initially, screening experiments were performed to enumerate the power density requirement for proper coupling of the laser beam in Gaussian as well as Donut beam profile, effect of shielding gas (He, Ar, and without shielding gas) flow rate, and welding speed which can yield stable keyhole, smooth weld surface and minimum weld defects (porosity, under bead, etc.). From the butt welded specimen, weldability of the alloy was studied in terms of joint strength, formability, fatigue and corrosion behaviour. The weld structure was verified with peak temperature and thermal profile analysis. The effect of the additional laser weld pass (bead on bead/remelting) on the existing butt weld was also studied by comparing the results of hardness, tensile tests, formability, fatigue test and corrosion study

From the detailed characterization it was observed that with a particular process window only coupling of the laser with the material was possible and Helium showed best result compared to other shielding gas conditions used in the study. The microstructures revealed defect free welds and hardness data confirmed presence of heat affected zone (HAZ) and huge drop in overall hardness after welding. After post weld treatment (aging cycle) the hardness was increased marginally but base hardness could not be achieved and double bead weld showed marginally higher hardness due to finer structure. In both single and double pass welds sharp drop in tensile strength were observed due to cast structure, not availability of age hardening effect and possible micro porosity. Formability value of the welds was low compared to the

base material due to the thermal strain in the welds. Thermal profile experienced by the material during welding was calculated and it revealed that the mechanical properties of the material decreased due to temperature experienced by the material leads to loss of aging properties of the material. The fatigue lives of the double pass welds were marginally high compared to the single pass welds due its finer structure and residual stress condition. In case of potentio-dynamic corrosion tests the welds showed poor properties due to presence of dendritic structure, but the double pass weld showed marginally better result due to its favourable residual stress level.

Key words: AA 6061-T6, Laser Welding, Numerical model, Shielding gas, High Cycle Fatigue, Corrosion, Formability.

Chapter 1: INTRODUCTION

1.1 Background

Aluminium alloys are the candidate materials for automobile and aircraft industry since 1930. In general, aviation industry completely is dependent on 2xxx and 7xxx aluminium alloys [1], however other alloys are also used in railway vehicles, bridges, offshore structural topsides and high speed ships due to its physical and mechanical properties such as light weight and high strength to weight ratio [2]. From last few years 6xxx series aluminium alloy has become a material of interest to both aviation industry for fuselage skins and automobile industry for body panels and bumpers because of their good strength, formability, medium weldability and high corrosion resistance [3]. In automobile industry most of the applications are sheet based; and these are conventionally joined by riveting. Major Disadvantages of riveting are extra weight to the structure, stress concentration, crevices corrosion and loosening due to vibrations. Moreover, it is a time consuming and manpower intense task. Thus, conventional welding took the place of reveting which in-turn decreases the weight of the vehicles and increases their fuel efficiency; and more over reduces the CO_2 emission [4].

During welding of aluminium alloys it has to overcome some challenges due to its physical properties such as tenacious oxide layer, high thermal conductivity, high coefficient of thermal expansion, solidification shrinkage and above all high solubility of hydrogen gases in molten state. Apart from these, liquation cracking and softening or property degradation in the heat affected zone and partially melted zone [5-6] are the other problems. Softening is one of the major concerns of 6xxx alloy [6-11] and besides softening behaviour in the weld fusion zone and heat affected zones, hot cracking is also an issue. Conventional processes like gas tungsten arc welding (GTAW) and gas metal arc welding (GMAW) are preferred for joining aluminium alloys.

During conventional arc process the heat of welding can results in melting of low melting phases which leads to hot cracking in the fusion zone (FZ) and heat affected zone (HAZ) [12, 13]. Arc welding process deteriorates the mechanical properties of the welded joint due to its high heat input nature [14]. To improve mechanical properties of the welded alloys, employment of low and concentrated heat input process is necessary which can cause increased joint efficiency by virtue of grain refinement in the fusion zone, reduced width of

heat affected zone, less distortion, control of segregation, reduced hot cracking sensitivity and reduced residual stresses. To reduce the heat input on the material, laser can be chosen as a tool for joining of Aluminium alloys.

Laser welding of aluminium alloy is in growing demand in industries for various structural and automotive applications. Recently laser welding was employed for A318 aeroplane and Audi, [15, 16]. Despite of some disadvantages like high reflectivity to the laser light, high thermal conductivity, low viscosity in the molten state, low vaporization temperature; still laser can be used by carefully selecting the process parameters. As example, once keyhole is formed, reflectivity problem can easily be overcome [17, 18].

Automotive aluminium alloys are either solid solution strengthened such as Al-5xxx (contains magnesium) or precipitation strengthened such as Al-6xxx (contains Mg_2Si). Loss of magnesium during the laser welding of Al-5xxx and Al-6xxx alloys may affect the degree of the mechanical properties of these alloys. The change in weld metal composition depends on the vaporization rate and the volume of the weld pool. Although the rate of vaporization increases with laser power, the change in composition is pronounced even at low powers if small spot size is used, due to the high surface to volume ratio of the weld pool [19]. Solidification cracking is a major concern during laser welding of aluminium alloys especially during pulsed laser welding. Most of the Al-5xxx alloys can be welded autogenously using a continuous wave laser beam with no solidification cracking [20].

Apart from these common problems of laser welding of Aluminium alloys which can be solved by selecting proper welding parameters, retention of the temper condition of such alloy is also a challenge. As AA 6061 alloys are used in different temper condition in actual applications, some welding process which can be employed directly without the need of any post welding heat treatment are of immense importance [21].

1.2 Motivation

The motivation of the present work comes from the possibility of realizing laser welding of 6061-T6 Al alloy and further improvement in mechanical properties of the weld by double bead technique so that the alloy can be used in as welded condition. This can also bring large by eliminating post welding heat treatment of the structure.

1.3 Problem Definition

The present study is focused on improving metallurgical and mechanical characteristics of 6061-T6 (solution heat treated + artificially aged) Al-alloy sheet butt welds obtained by common single pass CO_2 laser by refining the microstructure with extra laser pass/remelting. As laser welding of Al-alloy is a tricky job, every process parameters are to be optimised to achieve this goal and resultant welds have to characterized fully. Thus the problem may be divided as the following objectives:

- To study CO_2 laser coupling behaviour with the aluminium alloy.
- To optimise the laser welding parameters for 2 mm thick sheet of AA 6061-T6.
- To investigate the effect of shielding gas on laser welding of AA 6061-T6
- To examine the effect of double pass laser welding over single pass laser by mechanical and metallurgical characterizations.
- To investigate the microstructural, mechanical and electro-chemical properties of double and single pass welds.
- To justify the result with the thermal profile experienced by the weld during laser welding.
- To study overall weldability of this alloy.

1.4 Outline of the Thesis

The thesis comprises of five chapters. Significance of the problem taken up is discussed in Chapter-1, Introduction. Literature background related to laser welding of aluminium alloys is incorporated in Chapter-2. Details of various experimental procedures related to laser welding, microstructure analysis, hardness, tensile and high cycle fatigue test etc. are discussed in Chapter-3. The results obtained from the experimental investigations along with detailed discussion are incoporated in Chapter-4 and Chapter-5. Chapter-4 deals with effect of Laser Welding Parameter on Single Bead Welds and Chapter-5 represents the results of Bead over Bead Welds (double pass/remelting). Conclusions drawn from the present work are summarized in Chapter-6. Details of all the references cited throughout the thesis are compiled at the end in reference section.

Chapter 2: LITERATURE REVIEW

2.1 Introduction to LASER

The LASER is an acronym for Light Amplification by Stimulated Emission of Radiation, which has a wave length ranging from Ultraviolet (100-400nm) to Infrared (750nm to 1mm). Laser output can be delivered with very low (mW) to extremely high (1-100kW) power level. Laser has many special characteristics by which it has gained scientific and technological importance. Some of them are discussed here:

*Monochromatic***:** Laser is mono chromatic in nature, *i.e.* it is of a particular wave length in contrast to ordinary white light which is a combination of different wavelengths.

Directional: laser source emit light which is highly directional and relatively narrow in nature as compared to diffused sunlight.

Coherent: The light of a laser is said to be coherent, which means the wavelengths of the laser light are in phase in space and time.

These properties of laser make it more power concentric which is highly advantageous but at the same time more hazardous than any other ordinary light. Laser can be focused to a very small area with small interaction/pulse time (10^{-3} to 10^{-15} sec) on any kind of substrate through different medium. As a result, laser has wide applications, starting from metrology (Length/Velocity), Entertainment (laser show), Surgery/Therapy, optical communication/ computation, printer and pointer to heavy industry (melting etc.)

Applications

Based on the power, laser applications can broadly be divided in to 2 types.

Low power applications:

- Communication (data storage)
- Reprography (printing, scanning)

High power applications:

- Chemical (isotopes separations)
- Medical (skin, dental, eye surgeries)
- Heat source (rapid prototyping, material processing)

2.1.1 Generation of LASER

Laser is a coherent and amplified beam of electromagnetic radiation. The key elements in making laser a practical is its amplification achieved by stimulated emission due to the incident photons of high energy. Laser comprises there principal components, namely *Lasing medium:* a substance that when excited by energy emits light in all directions. The substance can be a gas, liquid or semi conducting material. *Excitation mechanism*: The excitation mechanism of a laser is the source of energy used to excite the lasing medium. Excitation mechanisms typically used are electricity from a power supply and flash tubes. *Optical cavity:* The optical cavity is used to reflect light from the lasing medium back into itself. It typically consists of two mirrors, one is fully reflected and other is partially reflected, these are at each ends of the lasing medium, as shown in the figure 2.1.

As the light is bounced between the two mirrors, it increases itself in strength, resulting in amplification of the energy from the excitation mechanism in the form of light. The output coupler of a laser is usually used to leave the optical cavity to be used for the production of laser beam. The chemical species (e.g.CO_2) in the gain medium determines the wavelength of the optical output. Between the two mirrors, one is a fully reflecting and the other a partially reflecting one. From the quantum mechanical principle, when an external energy is supplied to an atom, the irradiated atom attains an excited state. The excited atom returns to the ground state from the higher energy state by emitting the energy difference as a photon of frequency.

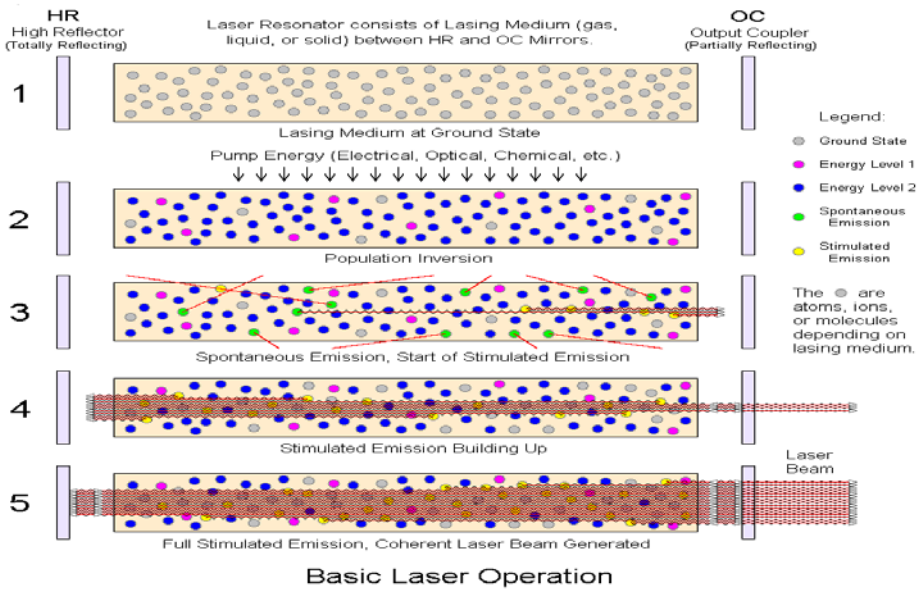

Fig. 2.1: Schematic Setup of Laser.

$$\gamma = \left(\frac{E_2 - E_1}{h}\right) \quad \text{.....2.1}$$

Where '*h*' is the plank's constant, γ is frequency of the radiation, E_1 is lower energy state, E_2 is higher energy state.

This phenomenon is known as *spontaneous emission* and a spontaneously emitted photon may in turn excite another atom and stimulate it to a photon by de-exciting it to a lower energy level. This process is called *stimulated emission* of radiation [22]. The latter is coherent with the stimulating radiation so that the wavelength, phase and polarization between the two are identical. A photon interacting with an unexcited atom may get absorbed by it and excite it to higher energy state. This situation, called *population inversion* is created by the pumping source. The photons moving along the optic axis interact with a large number of excited atoms, stimulate them and by this process get amplified. They are reflected back and forth by the resonator mirror and pass through the excited medium creating more photons. In each such round trip a percentage of these photons exit through the partially transmitting mirror as intense laser beam as shown in figure 2.1. Finally the laser beam is either guided on to the work piece by using reflecting mirrors or delivered at the desired site through optical fibres.

For example the Nd-Yag laser transmission is shown in figure 2.2. The laser was guided using reflecting mirrors, lenses and fibres.

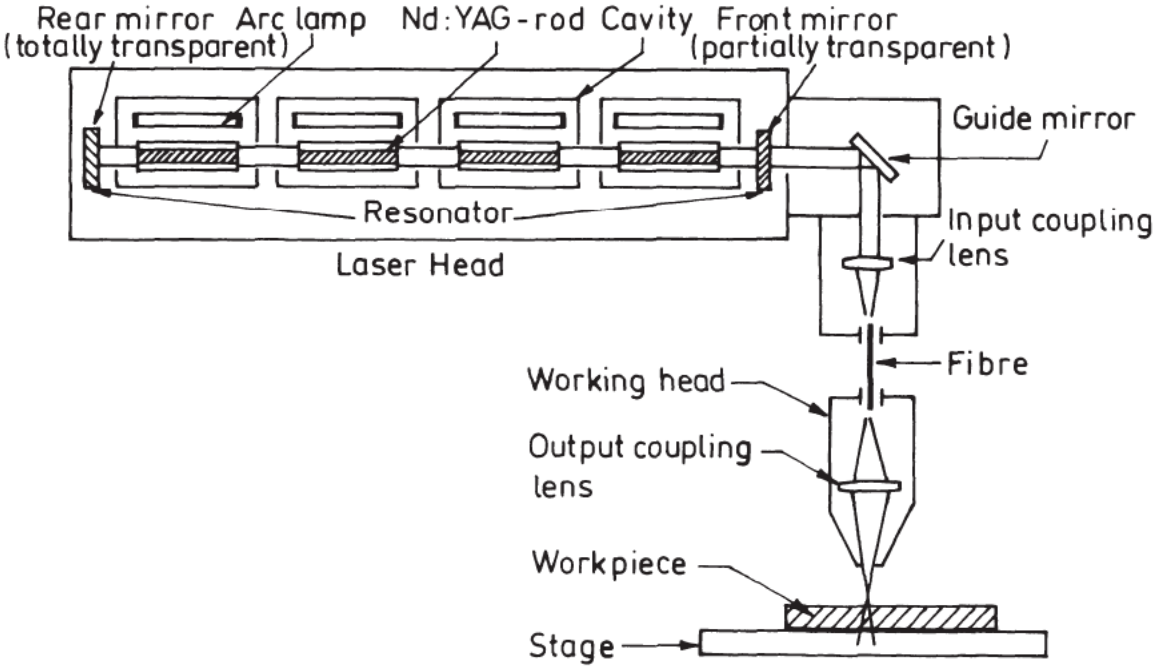

Fig. 2.2: Schematic set up of solid state Nd-YAG Laser with optical fibre Transmission system [23].

2.2 Laser Welding

Laser welding is a non-contact fusion welding process which involves melting and joining of two similar/dissimilar materials by the applications of heat generated by a fine focused spot of laser beam. One of the earliest and most widely practiced applications of laser material processing was joining of metallic sheets using a continuous wave laser. Now-a-days the automobile (Audi A2), aerospace (A318) and marine industry relies on lasers for a clean non-contact source of heating and fusion for joining of sheets [15]. More than any other conventional process, laser joining is applicable to inorganic/organic and similar/dissimilar materials with an extremely high precision, versatility and productivity of that can only be matched with electron beam welding. Unlike electron beam welding, laser beams are not affected by magnetic fields and joints are not required to be there in vacuum chamber [24, 25]. Laser welding can be performed with or without filler material, in various environments

(vacuum, air, pressurized chambers, or controlled atmospheres) and in some locations which are normally inaccessible or accessible only from one side. In addition to simple linear welds the latest laser welding facilities are capable of performing complex angular and curvilinear (non-linear) welds. Moreover, multi beam techniques are easily realized in laser welding. In comparison to conventional / arc welding, laser welding scores several advantages like high depth to width ratio, narrow weld widths with controlled bead size, faster welding with a higher productivity, less distortion due to small spot size, narrow heat affected zone, amenability to welding Al/Mg alloys and dissimilar materials and minimum contamination. These advantages come from its high power density at the work piece which is crucial to achieve keyhole welding. To control the formation of welds for a good weld quality the combination of the output power, welding speed, focal position, shielding gas and position accuracy should be correctly selected. Schematic representation of laser welding is shown in figure 2.3.

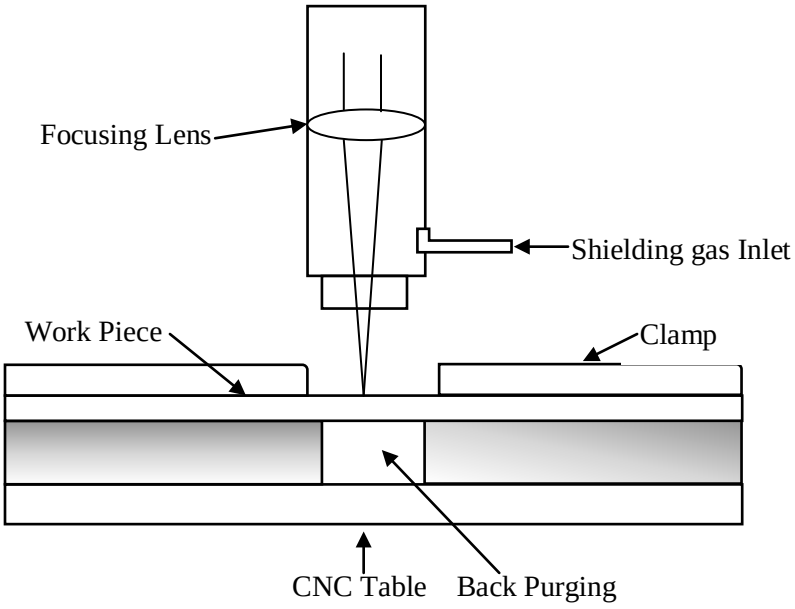

Fig. 2.3: Schematic Representation of laser welding.

The effectiveness of laser welding depends greatly on the physical properties of the material to be welded like absorptivity of laser beams, thermal conductivity, coefficient of thermal expansion, melting and boiling temperatures, wide solidification constituents and surface tension effect. Shorter wavelength Nd-YAG Laser has high absorptivity and thus less power

is required with the Nd-YAG laser than CO_2. At the same output power, smaller spot size means higher power density but the welds may become narrower than necessary or even not fully fused [26]. Laser welding seams are usually less than one quarter of the width of a tungsten-arc inert gas weld (TIG) for the same material thickness. Joint fit-up and beam alignment are more critical for a small spot size as small spot size may also lead to more loss of elements by vaporization causing undercut and under fill defects due to high power density. Thus small spot size cannot ensure good welding performance for Nd: YAG laser beam.

The position of focal points has an important influence on welding process and quality. The focal plane should be set where the maximum penetration depths or best process tolerances are produced. Focal position on the work piece surface produces smallest weld width while any deviation (above or below the surface) leads to wider welds [15].

The penetration depth and weld width both decrease linearly with increasing welding speed in general. Decrease in welding speed will lead to little increase in penetration depth but in turn will increase weld width and Heat affected zone (HAZ). Too high welding speed can increases the brittleness of the fusion zone in selected materials [27].

The surface condition of material influence the energy absorption of incident laser beam as well as the threshold power density for keyhole welding. Nearly 100% absorptivity can be obtained after the formation of keyholes due to reflections in the keyhole [28].

Modes of Laser Welding

Laser beams can be focused to a spot size of 0.1 mm to 13 mm, though only smaller sizes are used for welding due to high power density. The size of the focused beam at a given power dictates the power density of the laser at a given workplace. In laser welding, power densities should be high enough to either melt the material at the weld joint (conduction welding) or vaporize the material partially at the weld (keyhole welding) [22]. In case of keyhole welding as the work piece moves relative to the beam, vaporized or molten material solidifies behind the laser-material interaction zone to from a weld.

The most commonly used Industrial welding lasers are CO_2, Nd-YAG and Diode Laser and are used depending upon economics, welding speed, penetration requirements and the

material. Since the advent of fibre optics for laser beam delivery, flexibility also comes into play. In welding, one is often concerned about performing the process with minimum possible amount of heat. Different types of laser welding techniques are discussed below:

Conduction Mode Laser Welding

This welding technique offers less perturbation to the system because the laser radiation does not penetrate to the material being welded and the surface of the material remains unbroken. As a result the conduction welds are less susceptible to gas entrapment during welding. As mentioned above conduction welding is less efficient as it faces a primary loss of energy by reflection. Once energy is absorbed, surface is melted and the depth of melting is limited by the conduction of the energy to the subsurface and hence called conduction limited welding. Fig. 2.4 (a) shows schematic conduction weld melt pool [22].

Key Hole Laser Welding

In deep penetration or keyhole welding, there is sufficient energy/unit length to cause evaporation and hence, a hole forms in the melt pool. The 'keyhole' behaves like an optical black body as when the radiation enters the hole, it is subjected to multiple reflections before being able to escape. The hole is traversed along the joint with the molten metal ahead of the keyhole flow along the sides of the keyhole and solidifying at the back. To perform keyhole welding, a laser beam having a power density $>10^6$ W/cm^2 is focused on the surface of the metal work piece. The transition from conduction mode to deep penetration mode occurs with the increase in laser intensity and duration of laser pulse applied to the work piece. Welding efficiency can be defined as a power (or energy) transfer coefficient (η) where η is the ratio between laser power absorbed by the work piece and incident laser power. η is usually very small for conduction welding but can approach unity once a keyhole has been established. Schematic diagram of deep penetration keyhole mode is shown in figure 2.4 (b).

A part from the different modes, laser power, welding speed, defocusing distance and the type of shielding gas combinations should be carefully selected, so that weld joints having complete penetration, minimum fusion zone size and acceptable weld profile are produced.

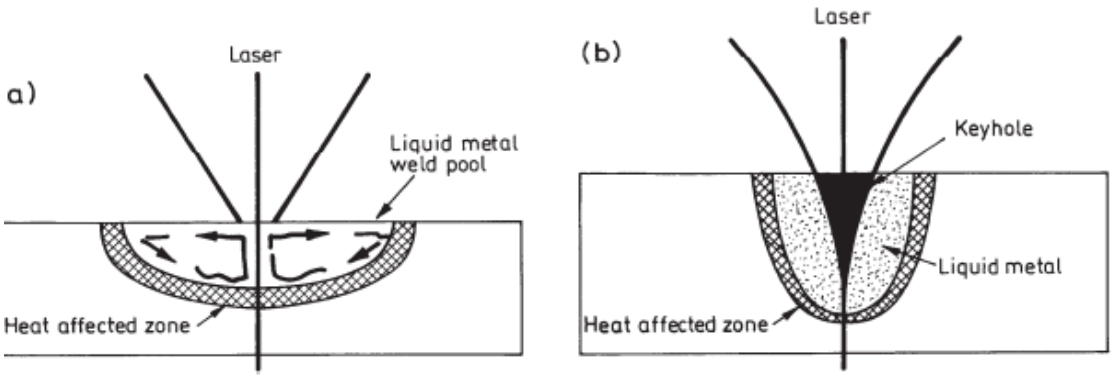

Fig. 2.4: (a) Conduction melt pool (semi-circular) (b) deep-penetration (key hole) welding [22].

Advantages of Laser Welding

- Good quality : narrow and deep weld seam
- High processing speed
- Low but concentrated heat input, which results in low and predictable distortion levels.
- Reduced post weld reworks.
- No mechanical contact between the laser equipment and the work pieces
- Rapid start and stop
- Welds at atmospheric pressure
- Easy to automate
- Joining of widely dissimilar materials is possible

Disadvantages of Laser Welding

- Poor gap bridging ability, which leads to high requirements on joint preparation
- High reflective materials are difficult to weld
- Loss of volatile elements
- High cost of equipment and maintenance

2.3 Aluminium Alloys

Aluminium alloys are categorised under most common non-ferrous alloys, one of the heavily consumed metal in the world right after the steel due to its attractive combination of physical

and mechanical properties [29-31]. A number of aluminium alloys have been developed to cater the needs of different industrial and engineering applications like automobile, aviation, marine, and enormous varieties of other products that we come across in everyday living [32]. Due to the modern environmental policy and fuel scarcity every automobile industry is looking forward to decrease the weight of the vehicles which would decrease the fuel consumption and in turn increase the efficiency of the motor vehicles [33]. In case of aerospace applications, after costly Titanium alloys, Al alloys are the only possibilities when metallic structure is needed. A unique combination of properties (light weight, high-strength-to-weight ratio, good corrosion resistance, excellent thermal and electrical conductivities, non-magnetic character, suitability for low temperature applications because of its FCC crystal structure) makes aluminium and its alloys one of the most versatile and economically attractive metallic material for a broad range of uses, from soft, highly ductile wrapping foil to the most demanding engineering applications [34-35]. Pure aluminium can be readily alloyed with many other metals to produce a wide range of physical and mechanical properties and this required to increase the strength of soft aluminium.

There are a variety of aluminium alloys which are in commercial use today and those can be classified into: 1xxx (commercially pure aluminium), 2xxx (Al-Cu alloys), 3xxx (Al-Mn alloys) 4xxx (Al-Si alloys), (5xxx Al-Mg alloys) 6xxx (Al-Mg-Si alloys), and 7xxx (Al-Zn-Mg) series. Among these, 2xxx, 6xxx, 7xxx are precipitation hardenable and can be processed to high strength levels. Wrought aluminium alloys are generally designated by using a four digit numbering system, originally proposed by the aluminium association of America . In this designation system, the first digit (Xxxx) indicates the principal alloying elements, the second digit (xXxx), if different from 0, indicates a modification of the specific alloy. The third and fourth digits (xxXX) are arbitrary numbers given to identify a specific alloy in the series. For instance in the alloy 5183, the number indicates that it is of the Al-Mg alloy series the 1 indicates that it is the 1st modification to the originally alloy 5083, and the 83 identifies it in the 5xxx series [36].

Aluminium alloys are used in different tempers depending upon the application requirements. The temper designation is always presented immediately following the alloy designation, with a hyphen between the designation and the temper (for example AA6061–T6) the first

character in the temper designation is a capital letter indicating the general class of treatment. The designations are defined and described as follows: F-as fabricated, O-annealed, H-Strain hardened, W-Solution treated, T-Thermally treated to produce stable tempers other than F, O, or H. The first number following the letter (basic Temper) indicates the specific combination of basic operations. In heat treatable aluminium alloys, some of the commonly used tempers are T3 (solution heat treated cold worked and naturally aged), T4 (solution heat treated and naturally aged), T6 (solution heat treated and artificially aged to peak hardness) T7 (solution heat treated and overaged), and T8 (solution heat treated, cold worked and artificially aged to peak hardness) [36].

Al-Mg-Si alloy 6061

The base material used in the present investigation was Al-Mg-Si alloy 6061 which is widely used in aerospace sheet metal structures. Alloy 6061 is a heat-treatable aluminium alloy used in structural applications; Alloy 6061 is normally used in T4 and T6 conditions. The base material is generally solution heat treated at 500°C followed by quenching and subsequent aging, either at room temperature for T4 temper, or aging at 170°C up to 18 h for T6 temper.

Thermo Physical Properties of Aluminium Alloy 6061 (T6)[37]

Density	2713, kg/m³
Specific heat	0.896 J/g.°C
Thermal conductivity	167 W/(m².K),
Electrical conductivity	43 (% IACS)

Mechanical Properties:

Yield strength	255 MPa,
Ultimate tensile strength	310 MPa,
Elongation at fracture	12%
Shear strength	207 MPa
Vickers Hardness	110 HV

2.4 Weldability of Aluminium Alloy

From the literature it can be observed that the welding of aluminium alloys can give rise to major issues/concerns like I) Hydrogen gas porosity, II) Solidification cracking, III) Liquation cracking in the HAZ and/or partially melted zone (PMZ), IV) Softening or Property degradation in the HAZ and/or PMZ and V) Inferior weld mechanical properties.

Regardless of the welding process and aluminium alloy used it is essential that the process parameters are carefully screened to produce defect free welds. As example for minimizing hydrogen gas porosity defects, the base material and filler wire should thoroughly be cleaned just before the welding. Further, as process parameters strongly influence the severity of hot cracking/liquation and HAZ PMZ problems, these parameters should be optimized systematically taking into the account not only weld defects but also weld microstructures and mechanical properties.

Hot cracking is one of the major concerns in welding of aluminium alloys, certain alloys are also prone to liquation cracking in the HAZ and PMZ as well, and this is where choice of filler material is critical for conventional welding process. To address this issue, welding of high strength heat treatable aluminium alloys are welded with low strength non heat treatable filler wire which will compensate the weld composition. In addition to the above technique, pulsed mode is also used sometime. This not only increases the resistance for hot cracking but also decreases the grain size for some aluminium alloys [38].

Few aluminium alloys has serious HAZ liquation cracking issue, it is necessary to use low melting filler wire to ensure that during liquation cracking we can take advantage. Yet another issue in filler material selection is corrosion resistance. While certain filler wires offer satisfactory hot cracking resistance and weld mechanical properties, they suffer from inferior corrosion resistance. Overall filler material must be carefully chosen ensuring satisfactory solidification cracking resistance, weld mechanical properties and corrosion performance [39].

The response of HAZ in aluminium alloy welds is dependent of the base material temper. Both heat treatable alloys and non-heat treatable alloys suffer from a loss of strength in the HAZ in as welded condition. In cold worked non heat treatable alloys, annealing effects in the

HAZ account for the loss of strength. In the case of non-heat treatable alloys nothing can be done to recover the properties of HAZ. In heat treatable alloys coarsening of strengthening precipiates occur due to over aging during welding; post welding aging treatment directly cannot help recover the HAZ properties. This necessitates a full post weld solution treatment followed by aging which however is not practicable in all situations especially for large structures. For heat treatable aluminium alloys, welding in T4 conditions is considered a better strategy. In this case the HAZ does not get over aged significantly, satisfactory weld joint efficiency can be achieved after post weld natural or artificially aging treatments [40].

2.5 Laser Welding of Aluminium and Aluminium Alloys

Aluminium alloys have high reflectivity towards lasers and it is known that as the wavelength of the laser decreases the process stability and processing window increases in two factors: 1. Type of material, 2. Wavelength of the light or incident radiation. For example aluminium alloy is more absorptive to Nd-YAG wavelength compared to CO_2 wavelength, this means aluminium alloy is highly reflective to CO_2 wavelength compared to YAG wavelength [41]. One more example is alumina and zinc oxides are absorptive at different wavelengths. The reason is absorption of light is dependent on the band gap of the material to be irradiated, this means depending upon the band gap of a material it absorbs a particular wave length light/laser more. Some way to increases the absorptivity for CO_2 laser beams are to modify the surface of Al alloys by mechanical or chemical roughening or by deposition of various absorptive paint or coating or by anodizing and dyeing the aluminium surface. These methods have been tried with varying degree of success for instance [42], some absorptive low reflective coatings such as graphite have been developed but they are not recommended because they may cause porosity or cracking. A high power Nd-YAG beam can easily penetrate the surface oxides and produce consistent welds of Al alloys in the as-received condition so it is usually unnecessary to remove the oxide layer before welding. However, the porous oxide films absorbs moisture, especially over extended periods in high humidity; therefore some traditional techniques such as mechanical methods (scraping or shaving) or chemical etching are employed to remove oxide layer. Aluminium usually has continuous oxide layers on the work piece surface because of its high chemical affinity for

oxygen. The presence of oxide layers can increase the absorptivity for CO_2 but not for Nd-YAG beam [43-46].

[26] M.PASTOR et al. have investigated pore formation during laser welding in two aluminium alloys with an Nd-YAG laser. He has discussed that the pore formation would be due to keyhole instability, the instabilities are caused due to surface tension exceeds vapour pressure, as these projections occurs inside the keyhole. As this projection size increases and it affects the gravitational force on the liquid projection, the collapse of the keyhole and pore formation takes place.

[47] KATAYAMA et al. have studied the penetration characteristics and defects formation conditions of several aluminium alloys with two different lasers (Nd-YAG and CO_2). The study was mainly focused on explaining keyhole phenomenon and porosity formation. Katayama has reported that welding speed plays a major role in formation of porosity. As the welding speed was increased, keyhole become narrower and shallower bubbles became smaller, and consequently both the size and number of pores decreased. The amount of porosity was similar in YAG and CO_2 laser welding but the amount depends on type of nozzle used for shielding gas purging.

[48] AKIO HIROSE et al. have investigated on quantitatively evaluating hardness distributions and softened regions in the weld HAZ of 6061-T6 aluminium alloy for laser beam welding and Tungsten inert gas (TIG) welding. It was observed that the widths of FZ and HAZ were decreased in laser welding due to its concentrated energy density in small area. He has described the softening behaviour in HAZ that in turn decreases hardness based on the process model of kinetic equation for 6061-T6 aluminium alloy. Width of softened region in the HAZ has calculated with varying net power input and welding speeds and it was found from the results that a high energy density and high welding speed in laser beam welding results in significantly narrower softened regions but the width is insensitive to welding parameters in comparison with TIG welding.

[25] N.Q.WU et al. investigated tailor welded blanks of aluminium alloy 6061 using Nd-YAG laser. A new mechanism for the strength and ductility loss is found by means of triboscope, optical microscope and energy dispersive spectroscopy. Nano-Indentation test revealed that hardness at the partially melted zone was distributed in-homogenously. The hardness at the area adjacent to grain boundaries was lower than at the centre of grain. The microscopically in-homogenous distribution of hardness was responsible for the failure that took place at the partially melted zone.

[49] A.B.M. MUJIBUR RAHMAN et al. have studied galvanic corrosion of laser welded 6061 aluminium alloy and it was reported that different weldment regions contained different potentials. The weld fusion zone is found to be the most cathodic region of the weldment while the base material is the most anodic region. The rate of galvanic corrosion, controlled by the cathodic process at the weld fusion zone, increases with time until a steady state maximum is reached. On galvanic corrosion the corrosion potential of the weld fusion zone shifts in the positive direction and the free corrosion current increases. It was proposed by the author that the cathodic process at the weld fusion zone causes a local increase in *pH* that in turn causes dissolution of the surface film resulting in the loss of Al to solution and the increase of intermetallic phases. The increase in galvanic corrosion may result from either the build-up of the intermetallic phases in the surface layer and/or significant increase in surface area of the weld fusion zone due to the porous nature of the surface layer.

Chapter 3: EXPERIMENTAL WORK

3.1 Introduction

The main objective of this investigation is to realize satisfactory welds in both double and single pass welds of 2 mm thick AA6061 (in T6 condition) alloy and to characterize their microstructures and mechanical properties. Manufacturing/processing of the laser welded joints; their characterizations and structure property correlation study carried out in the present work have been outlined in Fig. 3.1. First for narrowing down the laser welding process window screening experiments were carried out as Bead on Plate (BOP) welding and at the same time shielding gas was optimised. After that, with the identified processes window, single pass welding was carried out in Donut mode. Separately, double bead laser welding was also carried out (Donut + Gaussian) and this was followed by characterizations of all the welds produced. Details of each process and characterization are elaborated in the subsequent sub sections.

3.2 Base material

2 mm thick sheets of 6061 Aluminium alloy in T6 (solution treated + artificially aged) condition was used in the present study. The nominal chemical composition of the base material is listed in the Table 3.1.

Table 3.1: Chemical composition of AA 6061 alloy (wt. %)

Si	Fe	Cu	Mn	Mg	Zn	Cr	Al
0.65	0.31	0.27	0.12	1.05	0.01	0.25	Balance

3.3 Sample Preparation

For the present study plates of the aluminium alloy of 2 mm thickness were cut into specimens of 150 mm X 100 mm size. The edges of the samples were mechanically ground to remove sharp edges and before welding, specimens were cleaned with stainless steel wire brush followed by acetone wash to remove oxide layer and dirt from the

surfaces of the specimen. These specimens were directly used for Bead on Plate experiments and for butt welding experiments two such pieces were joined without any joint preparation.

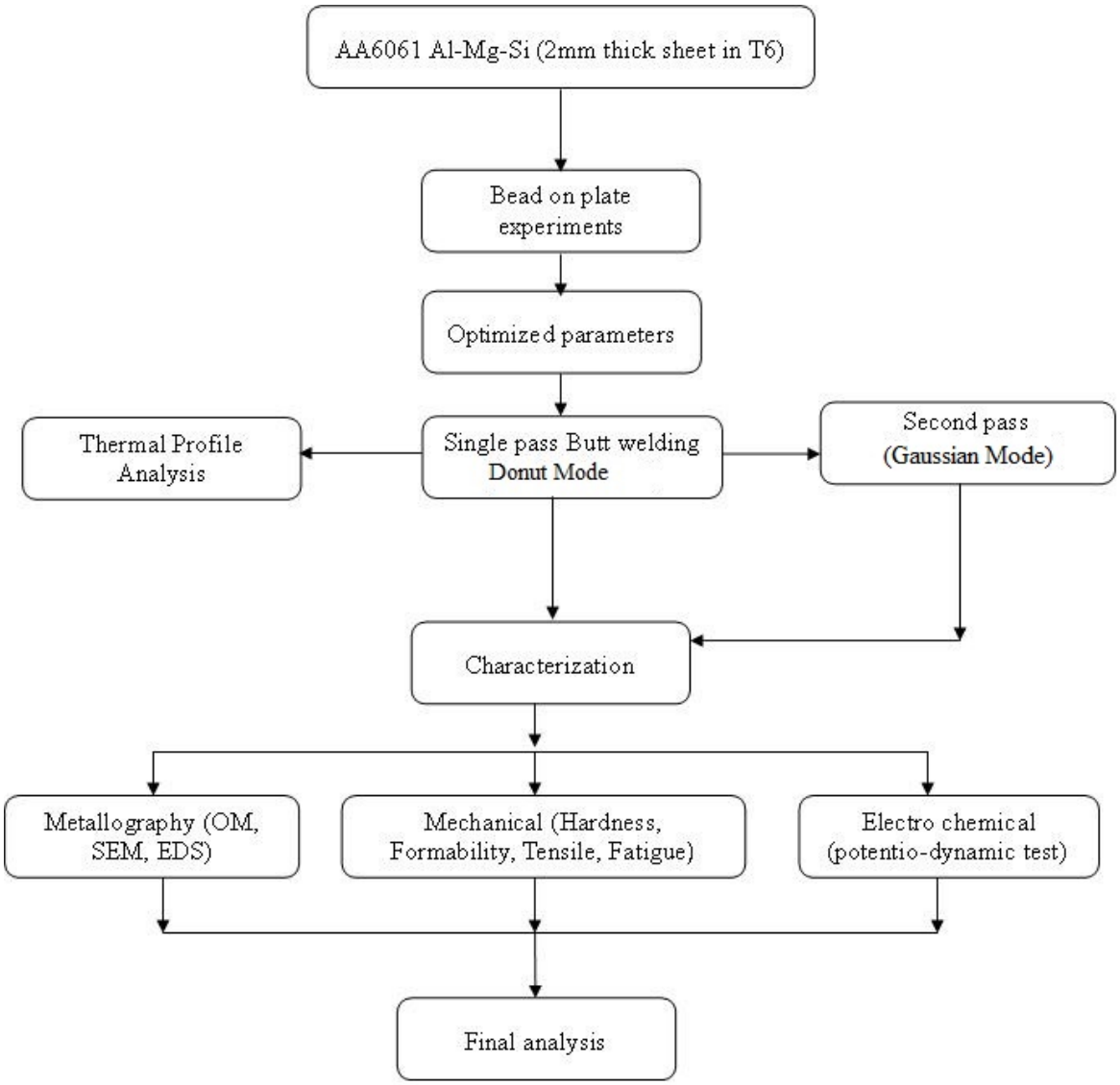

Fig. 3.1: Experimental plan

3.4 Welding Experiments

All the welding experiments were done using a commercially available 3 axis DC 035 slab CO_2 laser (Rofin Sinar). CO_2 laser has a slab like arrangement of electrodes and hence called slab CO_2 laser. The electrodes has a gap of 2 mm between them and lasing gas mixture is fed in gap and is maintained stationary unlike the conventional CO_2 laser. The

gases are excited by radio frequency discharge between the electrodes. The narrow inter-electrode spacing allows effective removal of the heat from the discharge chamber through the electrodes which are directly cooled by water. A small bottle is integrated into the laser head containing ready-made gas mixture which is needed to supply fresh laser gas only at certain intervals (approximately 72 hrs). The mixture in the bottle integrated into the laser head consist of Carbon dioxide, Nitrogen, Helium, xenon, krypton and Carbon monoxide. The laser beam is produced due high voltage input, the N_2 vibrates and it makes CO_2 to excite, the exited atoms are cooled due to cooling water supply. There are two mirrors namely the output mirrors and the rear mirror which act as an optical resonator. The laser beam is produced in the resonator and is then emitted behind the laser beam telescope. The laser has a near Gaussian beam quality ($K > 0.9$). External, water cooled, reflective beam shaping components are used to make sure that beam with a quality of $K > 0.9$ is obtained. This laser emits light with a wave length of 10.6 µm and possesses an overall efficiency of approximately 1-13%. This laser machine was attached to the workstation of a 4 axis CNC with maximum X, Y, Z stroke of 3000 mm, 1500 and 300 mm respectively.

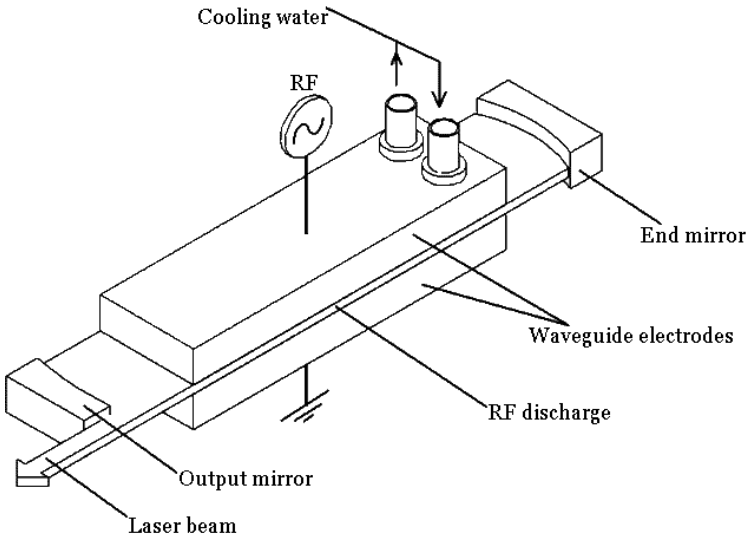

Fig. 3.2: Schematic of CO_2 slab laser.

The CO_2 slab laser unit was fitted with 300 mm focal mirror which can yield spot sizes of 360 µm in Donut mode, and 180µm in Gaussian beam mode. During laser experiments, the focal plane of the laser was positioned at the surface of the sheet. The shielding gases were fed through a 5 mm diameter nozzle in the trailing mode configuration at a gauge pressure of 1 bar and nozzle stand-off distance of 3 mm.

3.4.1 Screening Experiments

For screening of welding parameter Bead on Plate (BOP) experiments were carried out both in Donut and Gaussian mode. First, the effect of shielding gases was studied with Donut mode and after optimizing, He as the shielding gas with flow rate of 18 l/min was selected for Gaussian (BOP) experiments. Actually, BOP parameters given in Table 3.2 were chosen systematically after analysing the results obtained from each set of parameters, sequentially.

Table 3.2: Parameters for Bead on Plate welding

Sl. No	Laser Power (kW)	Speed (m/min)	Laser beam mode	Shielding gas – flow rate (l/min)
1	3.5	6, 5, 4, 3, 2, 1	Donut	Ar - 10,14,18,22 He – 10,14,18,22 No gas (without shielding)
2	3	6, 5, 4, 3, 2, 1	Donut	
3	2.5	1, 2	Donut	
4	2	1	Donut	
5	1	1	Donut	
6	3.5	6,5,4,3.5,3	Gaussian	He - 18
7	3	6, 5, 4, 3.5,3	Gaussian	
8	2.5	6,5,4,3.5,3	Gaussian	
9	2	1,2	Gaussian	
10	1	1	Gaussian	

3.4.2 Butt Welding Experiment

For the butt welding experiments parameters were selectively chosen from BOP experiments in terms of full depth of penetration, minimum fusion zone weld width, and minimal porosity and cracking which are discussed in details in subsequent chapters. Butt welding parameters which were employed here are tabulated in 3.3. The butt weld were produced from Donut mode for single pass weld and combination of Donut + Gaussian

mode for double pass welding. Before laying second bead the welds were cleaned with stainless steel wire brush to remove any blackish layer from the surface of the weld and followed by acetone wash. Immediately after cleaning, the second bead was laid on top of first bead. Donut beam at a 3.0 kW power and 4 m/min welding speed and Gaussian beam at a power of 2.5 kW and a weld speed of 6 m/min were chosen. For both single and double pass butt welds He was used as a shielding gas as per earlier optimization.

Table 3.3: Parameters for Butt Welding

Power (kW)	Speed (m/min)	Shielding gas (l/min)	No of Weld Pass
3	3.5	Ar-20	Single pass
3.0	4	He-18	
3	4.5	0-gas (without shielding)	
3.0(Donut Mode)+2.5 (Gaussian Mode)	4+6	He-18	Double pass

3.5 Post Welding Heat Treatment

The welded specimens were subjected to post weld heat treatment to check any possible age hardening phenomena. The treatment was carried out at 170^{o}C for 2, 4 and 6 hrs (holding) followed by quenching in water.

3.6 Characterisation of Welds

3.6.1 XRD analysis

The welded joints and the base material were subjected to XRD analysis using X-ray Diffractometer - Panalytical PW3040 X'Pert MPD, to check possible changes in phases during welding and post welding heat treatment. In order to study variation in residual stresses, welded joints and the base material were studied by 2-axis goniometer fitted XRD equipment (model: D8 DISCOVER DAVINCI, BRUKER, Germany).

3.6.2 Macro and Microstructural Examination

Coupons of 10 mm x 5 mm size were cut in the transverse direction from each welded samples for metallurgical characterization by using an abrasive cutter. Some of the cut samples were mounted to study the cross section of the welds. The mounted samples were polished using automatic polishing machine (Buhler) to obtain scratch free mirror finished metallographic surface. The polishing procedure of this alloy include polishing with 320-grade emery paper (10 min), followed by polishing with diamond suspension of 9 µm (10 min), 6 µm (10 min), 3 µm (10 min) & then by alumina suspension of 0.05 µm (10 min). The polished specimens were thoroughly cleaned with running water and alcohol. After cleaning the samples were ultrasonically cleaned with acetone for 25 min. The polished and cleaned samples were etched using a Keller's reagent (2.5 ml of Nitric acid, 1.5 ml of hydrochloric acid, 1 ml of hydrofluoric acid, and 95 ml of water) for 10 sec.

Macrostructure of the welds were studied using S2-E7 Olympus stereo zoom microscope at a magnification of 25X to obtain various bead geometry measurements like convexity, under bead, fusion zone (FZ) width etc. After macroscopic examination welds were analysed using optical microscope and scanning electron microscope (SEM). Optical microstructure of the welds were obtained using Olympus DP12 optical microscope at a magnification of 500x and SEM was done using Hitachi S3400 scanning electron microscope having Energy-dispersive X-ray spectroscopy (EDS) attachment.

3.6.3 Mechanical Characterization

Microhardness Study

Microhardness measurements were carried out across the welds on the mounted cross section. The hardness survey was carried out across the weld starting from the base material and proceeding up to the base material so as to cover all the regions such as Fusion zone, Heat affected zone and Base material. The microhardness measurements were carried out using an automatic UHL IMS 5.0-Vickers micro hardness tester fitted with a diamond indenter. A 50 gm load and dwell time for 15 sec were kept constant for all indentations and the distance between the two indents was maintained 150 µm in order to avoid possible effects of strain field caused by nearby indentation. An average of 3-4 indentations taken in identical locations was reported.

Tensile test

Tensile testing of butt joints and base material were carried out according to ASTM E8 sub size sample using an Instron 5584 machine with video extensometer attachment at a cross head speed of 1mm/min. At least 3 specimens were tested for each condition. The dimensions of the tensile specimens used in this study are shown in the Fig. 3.3. In case of butt welds the fusion zone was kept at the centre of the tensile specimen.

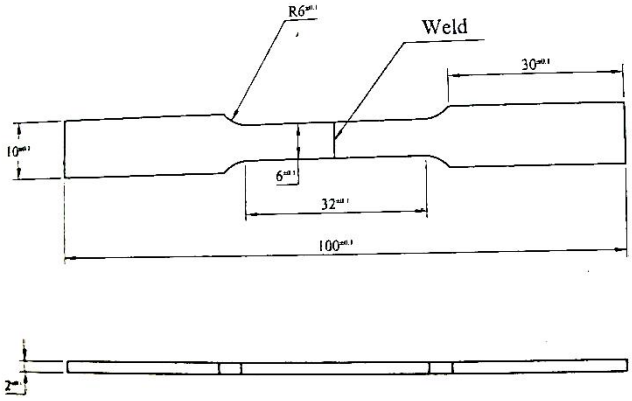

Fig. 3.3: Tensile specimen dimensions

Fatigue Testing

High cycle fatigue testing of welded samples and base material were carried out in Tension-Tension mode according to the standards. The Testing was carried out using 3kN Micro-Tensile Testing Machine-Series LFV. Hydraulic power pack –Type PAC -3, No-1048, high resolution video extensometer-Type-MC46 and digital control system, type-EDC580, No-0.0051. The specimens were mechanically ground to a thickness of 0.5 mm from 2 mm, to prevent Machine vibration. Tension-Tension cycling loading at a stress ratio of R=0.1 was applied with a frequency of 15 Hz of sinusoidal waveform and at least four specimens were tested at each strain amplitude. The dimensions of the fatigue specimens used in this study are shown in the Fig. 3.4. In case of butt welds the fusion zone was kept at the centre of the fatigue specimen.

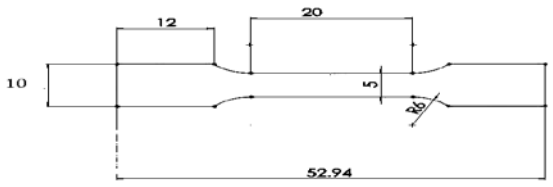

Fig. 3.4: Fatigue specimen dimension

Formability test

Formability study was performed by Erichsen cupping test both on welded coupons and base material to identify the change in ductility. It is a simple stretch forming test of a welded sheet clamped firmly between blank holders to prevent in-flow of sheet material into the deformation zone. The punch was forced onto the clamped sheet with tool contact (no lubrication) until crack was visible by naked eye and the linear movement of the punch was recorded as Erichsen Number or Erichsen Index (I.E.). Schematic of the experimental set up is shown in Fig. 3.5. In case of all the welded samples the punch was pushed from the bottom side of the weld.

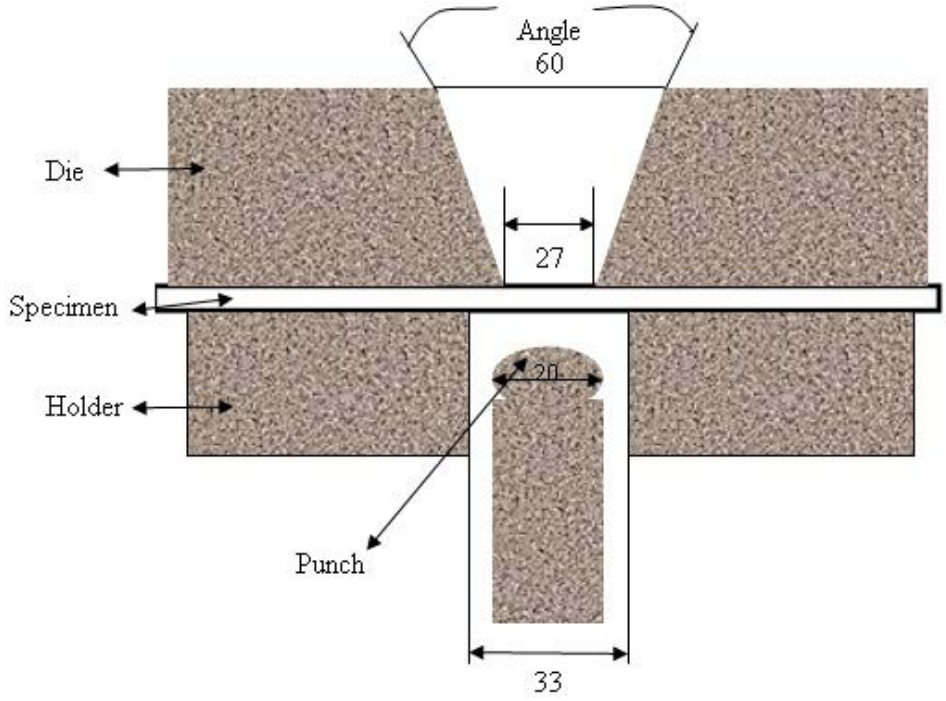

Fig. 3.5: Die and Punch design used in Erichsen formability test

3.7 Corrosion test

Base material and butt welded specimens are subjected to potentio-dynamic polarization test in a 3.6 wt % NaCl solution to study the mechanism and rate of anodic dissolution. For this, a PS6 Meinsberger Potentiostat/Galvanostat connected to a standard three electrode cell comprising the sample as the working electrode (WE), a saturated calomel reference electrode (RE) and a platinum counter electrode (CE) was used. Schematic of the experimental set up is shown in Fig.3.6.

After the corrosion experiments, specimens were subjected to SEM analysis to study the severity of corrosion damage.

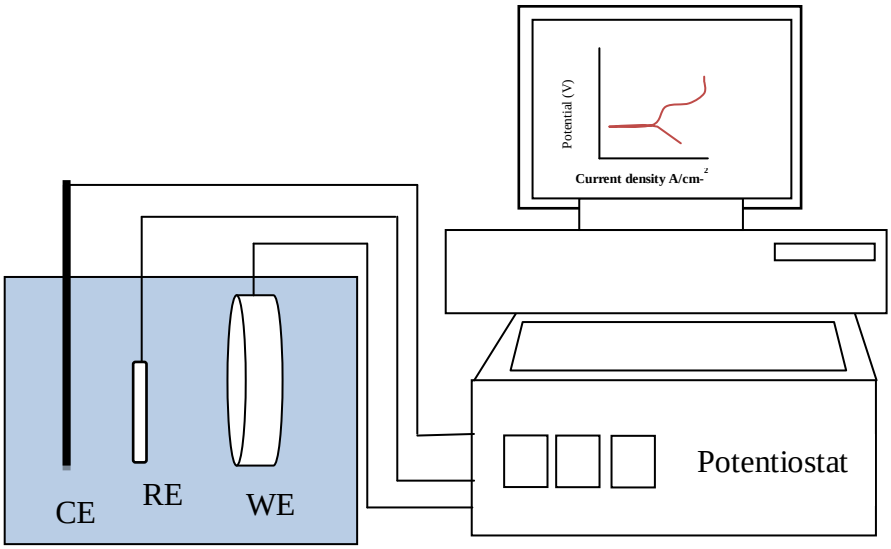

Fig. 3.6: Schematic of corrosion test setup

Chapter 4: EFFECT OF LASER WELDING PARAMETER ON SINGLE BEAD WELDS

4.1 Introduction

First bead on plate (BOP) experiments were carried out to narrowing down the process window by means of laser coupling observations. Experimenting over a wide range of laser and shielding gas parameters, successful process window obtained from BOP experiments was employed on actual butt welding experiments and resulting welds were characterized systematically.

A DC035 slab CO_2 laser (Rofin Sinar) fitted with 300 mm focal mirror which can yield spot sizes of 360 µm in donut mode, was used in this study. The focal plane of the laser was positioned at the surface of the sheet. Helium shielding gas was fed through a 5 mm diameter nozzle in the trailing mode configuration and nozzle standoff distance of 3 mm.

4.2 Effect of Welding Parameters in BOP Experiments

Fig. 4.1 shows the cross sectional macrostructures of some selected welds in terms of laser welding speed, laser power and shielding gas flow rate. These macrostructures show the typical wine glass shape which is often found in laser welding. The fusion zone (FZ) had a bright contrast compared to the base material. Heat affected Zone (HAZ) cannot be depicted by the macrostructure but from the hardness data it was confirmed later. It can be observed that with reduction of welding speed the penetration depth increases, moreover it expands the bead width due to increase in heat input. This may also cause loss of low melting alloying element such as Mg and low melting eutectics causing decreases in mechanical property of the material [50, 51]. In order to investigate the possible loss of alloying elements due to laser welding, on an existing weld line scan across different direction has been done using Energy Dispersive Spectroscopy. Fig. 4.2 shows such scan with 3 kW power, 3 m/min welding speed, 18 l/min flow rate of Helium shielding gas and in that no reduction in Mg and Si content was observed.

Laser Power (kW)	Welding Speed (m/min)	Shielding gas (Helium)		
		10 l/min	14 l/min	18 l/min
3	1	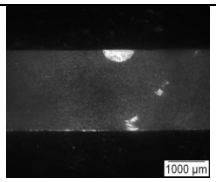	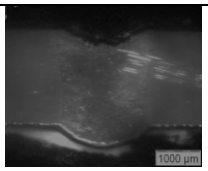	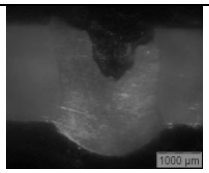
3	3	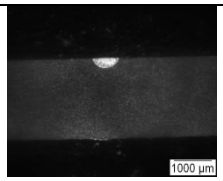	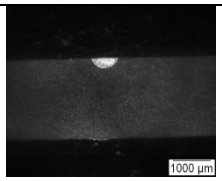	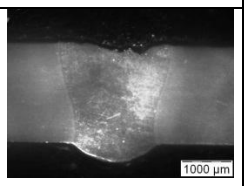
3	6	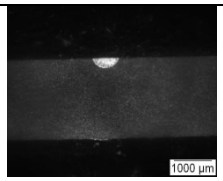	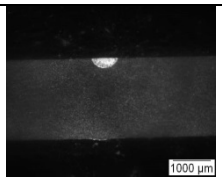	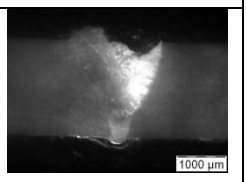
Laser Power (kW)	Welding Speed (m/min)	Shielding gas (Argon)		
		14 l/min	18 l/min	22 l/min
3	1	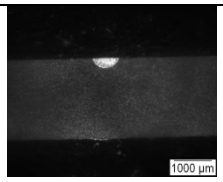	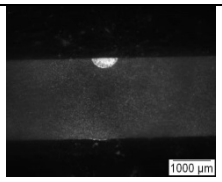	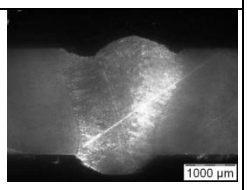
3	3	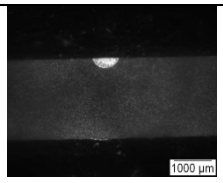	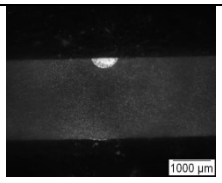	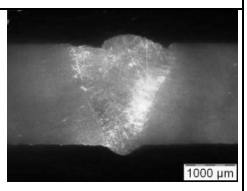
3	6	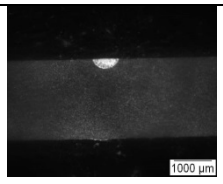	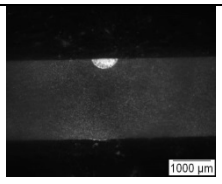	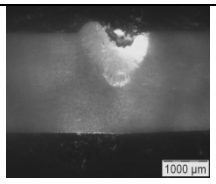
Laser Power (kW)	Welding Speed (m/min)	Without Shielding gas		
3	1		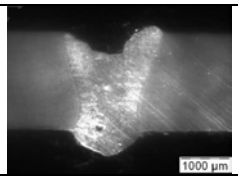	

3	3	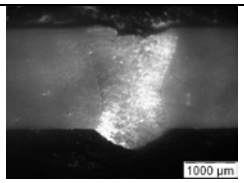	
3	6	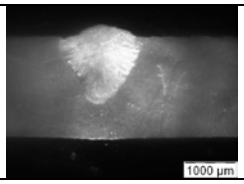	

Fig. 4.1: Effect of Laser parameters and shielding gas flow-rates on penetration

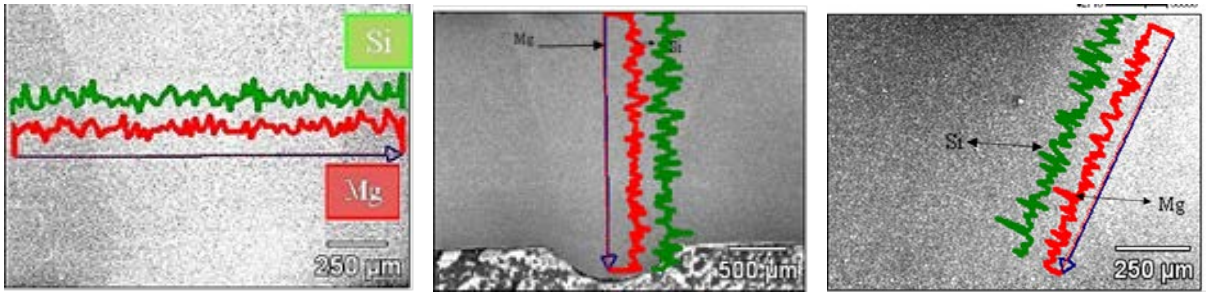

Fig. 4.2: EDS line scan on welds obtained with 3 kW power, 4 m/min welding speed and 18 l/min flow rate of helium shielding gas

Macrostructure of the welded joint also depends on the shielding gas used and its flow rate as it affects the molten pool, plasma generation and plasma plume behaviour. As in laser welding of Al-alloy plasma generation is high, in order to push plasma plume out of the weld, higher shielding gas flow rate is necessary specially in case of low density gas like He (0.1664-0.1785 kg/m^3) [52]. From Fig. 4.1 It can be observed that a flow rate of 10 l/min, it has partial penetration due to the formation of plasma plume above the weld. Optimizing such macrostructure in terms of proper penetration, absences of internal defects such as cracks, macro pores as revealed at this magnification (25X), it was found that 3 kW power, 4 m/min welding speed, 18 l/min flow rate of Helium shielding gas is a good choice. In case of argon as shielding gas 3kW power, 3.5 m/min welding speed, 22 l/min flow rate is the best possible parametric window for further processing. It can be observed that the bead width is more in case of helium as shielding gas compared to the Argon and this could be due to higher thermal conductivity of helium. It can be observed that the depth of penetration increases with decrease in welding speed due to the increase in heat input and the trend observed is in line with the known fact for any welding process. Bead width also exhibits similar trend. Quantitative value of these are discusses in later section.

Laser Coupling Behaviour

During BOP laser welding trials, from the appearance of the bead primary idea about extent of coupling can be obtained and for further study the cross sectional macrograph can be analysed. Fig. 4.3 shows distinct difference between a coupled and a non-coupled laser beam. It can clearly be observed that the coupled weld surface appears shiner than the one without coupling which appears dull.

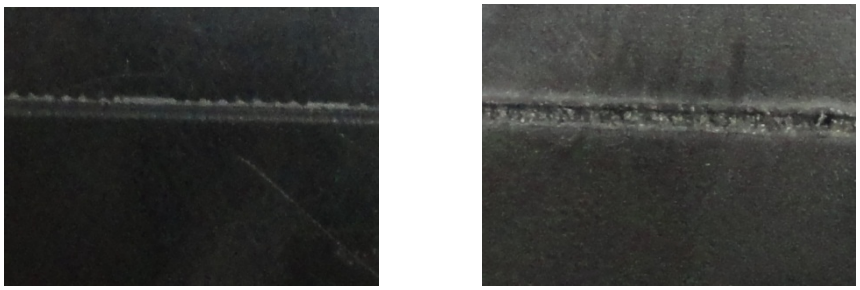

(a) (b)

Fig. 4.3: Coupling behaviour: (a) No Coupling and (b) Coupled

Laser coupling behaviour as observed during bead-on-plate welding with laser power and speed is demonstrated in Fig. 4.4. From the figure it is clear that there exists a minimum power level below which coupling cannot be achieved. Below such level the power is not sufficient to melt the surface for welding after compensating the losses like reflectivity, plasma formation etc. From the figure it can be observed that as the power density increases, the coupling efficiency also increases even with higher welding speed. At low flow rates and low welding speeds, there is higher chance of the plasma plume staying in the weld zone resulting in entrapment of the laser beam energy and insufficient laser energy intensity available for coupling with aluminium.

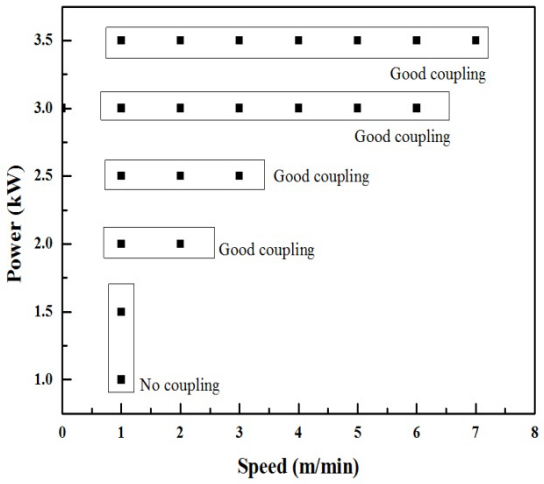

Fig. 4.4: Effect of welding speed on coupling behaviour

To enumerate the effect of shielding gas flow rates on coupling behaviour similar observations were carried out with varying gas flow rate of Helium and Argon and the same is shown in Fig. 4.5. From the figures it can be observed that shielding gas flow rate has significant effect on coupling behaviour during laser welding of 6061aluminium alloy. To get the laser coupled with the sample and to get good welds, the minimum requirement is low power with higher flow rate or with higher power and lower flow rates. Even up to 10-18 l/min flow rate of Ar or 10-16 l/min flow rate of He it did not couple at low welding speeds. During welding experiments metallic plumes were observed and as the welding speed was decreased, metallic plume moved around the front and back part of the weld. Requirement of lower flow rate of He is due to its higher ionization potential which helps in coupling by reducing the plasma plume formation.

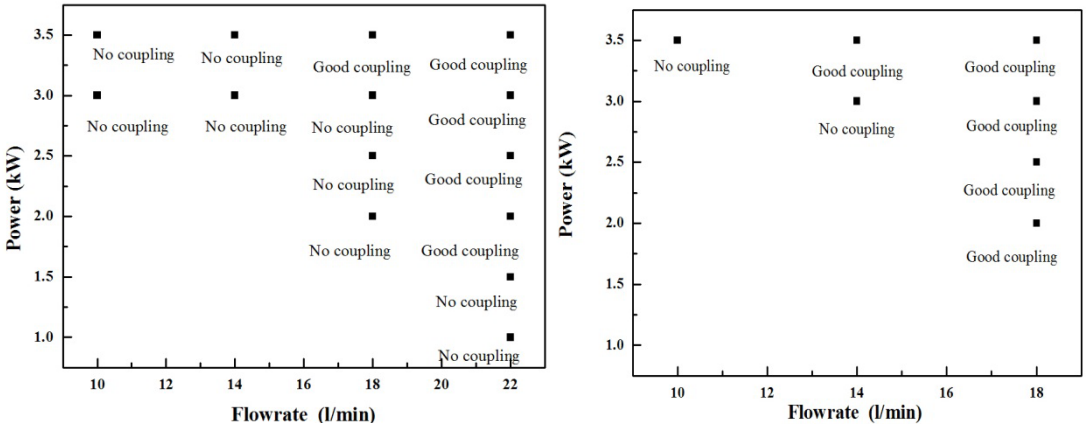

(a) (b)

Fig. 4.5: Coupling behaviour with (a) Argon and (b) Helium

Bead geometry analyses

The influence of various parameters used in the present study on the bead geometry values of the welds are shown in Fig 4.6. From the figure it can be observed that the depth of penetration increases with the decrease in welding speed in common due to the increase in heat input. The trend observed is in line with the known fact with any welding process that the depth of penetration increases with the heat input. Bead width also exhibited similar trend in all the shielding conditions. A dip in the width of the weld bead was observed when the depth of penetration changed from partial to full penetration (Fig. 4.6a, 4.6c). At the threshold value of heat input for achieving full penetration, the excess laser energy is lost through the bottom of the keyhole resulting in reduction of weld bead width.

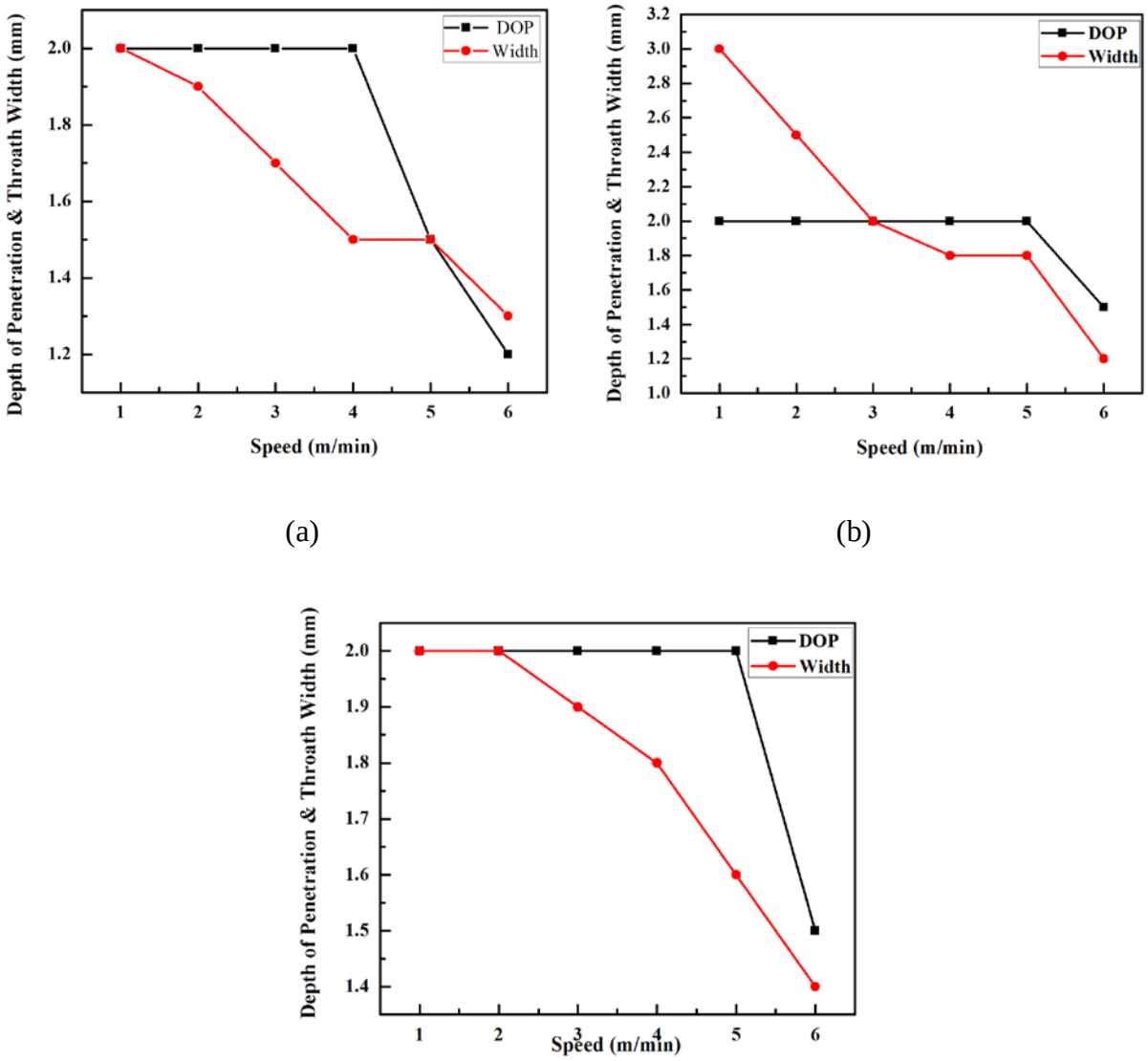

Fig. 4.6: Effect of shielding gas on the depth of penetration and throat width, (a) with Argon, (b) with Helium and (c) without shielding gas.

However, with further increase in laser energy beyond the threshold value the bead width continues to increase as the excess heat can be utilized in increasing the bead width. Among the three shielding conditions experimented, the overall trend shows that the highest depth of penetration is obtained with He. He has higher ionization potential and hence suppresses the plasma more effectively than Ar. Moreover helium has high thermal conductivity (0.142 W/m K), and due to this it increases the throat width also [53]. This reduces/avoids the loss of laser energy due to the absorption by plasma above the surface of the weldments thereby increasing the depth of penetration.

4.3 Laser Butt welding

The butt welding parameters screened from BOP experiments in terms of penetration, weld width and minimal porosity and cracking are shown in Table 4.1 and the same were discussed in details in Experimental work section. Single pass butt welding with these parameters were carried out in donut mode and the detailed analysis of the welds are presented in the subsequent sections. The butt welded specimens were also subjected to artificial aging treatment to check any possible change in strength.

Table 4.1: Parameters for butt welds

Sl.No	Power (kW)	Speed (m/min)	Shielding gas (l/min)
1	3	4.5	No gas (without shielding)
2	3	3.5	Ar-22
3	3	4	He-18

4.3.1 XRD analysis

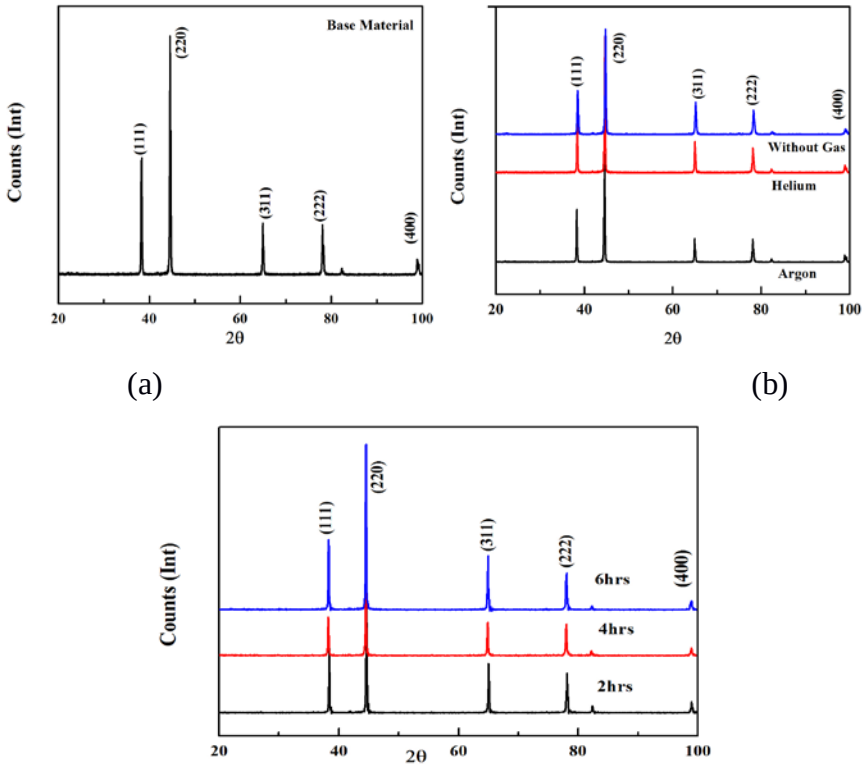

(a) (b)

(c)

Fig. 4.7: XRD plot of (a) base material, b) as welded condition (He-18 l/min, 3 kW Power, 4 m/min speed, Ar-22 l/min, 3 kW Power, 3.5 m/min speed, without shielding-3 kW Power,4.5 m/min speed) and (c) after post welding heat treatment of weld made with He (170^{o}C for 6 hrs)

The welds were subjected to XRD analysis to check possible changes in phases during welding and post welding heat treatment. Fig. 4.7 shows base material, welded condition and post heat treated condition XRD profile.

In all the profiles only peaks of α (Al-rich solution) are visible. In the base material (T6 condition) also the presence of precipitates could not be observed due to low fraction of those phases and this is a common observation of age hardenable alloys. So, from the XRD retention/formation of fine precipitation during welding or in post welding heat treatment could not be ascertained.

4.3.2 Macro and microstructural Analysis

Figure 4.8 shows macrostructure of butt welds with varying shielding gas conditions. The reasons for choosing these parameters for butt welds were the full depth of penetration and decrease in bead width that will in turn decrease the heat affected zone which was observed from screening experimental studies. The basic thought that was used is decrease in bead width could yield in better mechanical properties of the welds.

Laser Power (kW)	Welding Speed (m/min)	Shielding gas	
3	4.5	No gas	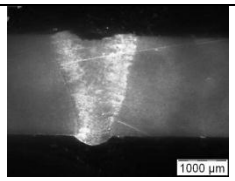
3	3.5	Argon (22l/min)	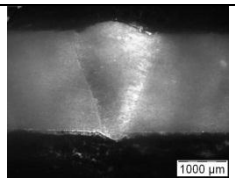
3	4	Helium (18l/min)	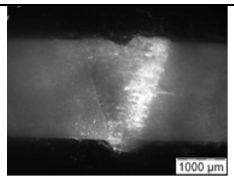

Fig. 4.8: Butt welds with varying shielding gas conditions

The microstructure of the base material is shown in Fig 4.9. The base material shows fine precipitates which are homogeneously distributed in the Al rich matrix.

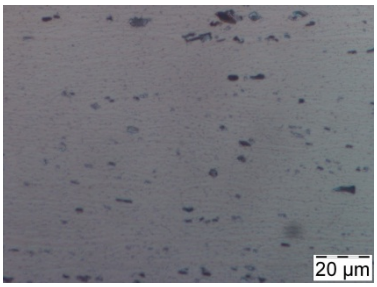

Fig. 4.9: Optical micrograph of Base Material (AA 6061 alloy)

Helium	Argon	Without Shielding
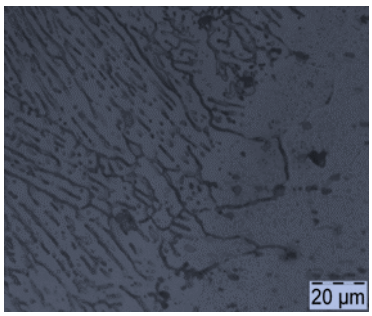 FZ and HAZ	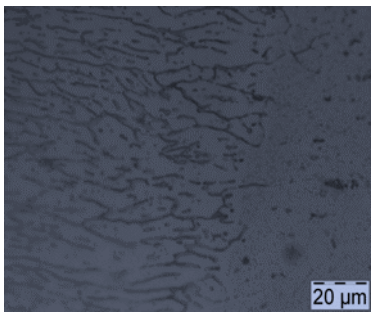 FZ and HAZ	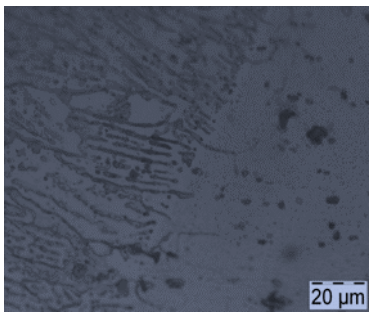 FZ and HAZ
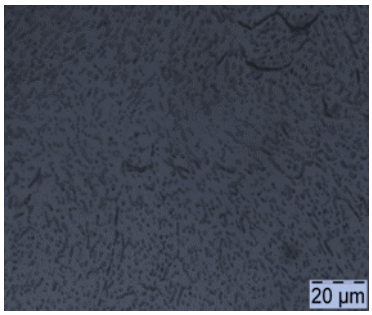 FZ	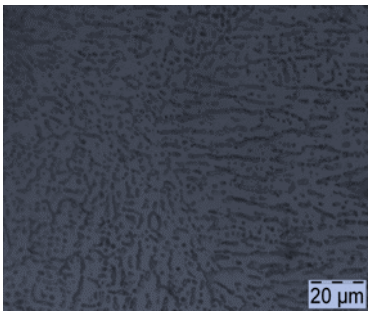 FZ	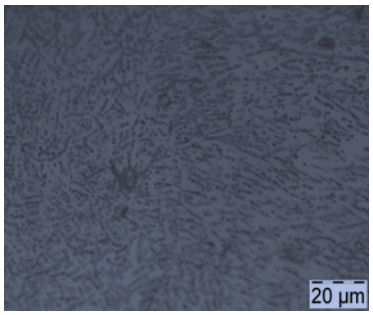 FZ

Fig. 4.10: Microstructures of welds with different shielding conditions

Fig. 4.10 shows optical micrographs of HAZ-Fusion line interface and fusion zone under different shielding conditions. From careful observation of Fig. 4.10, it can be seen that the microstructure of weld from base material to centre of the fusion zone was varying from cellular dendritic to parallel dendritic region and finally to narrow equiaxed dendritic region. Variation in microstructure can result from different cooling rates and heat flow that could have resulted in different region, and has been studied by Sindo Kou [10]. Adjacent to fusion line, towards the base material coarse grained structure was observed as heat affected zone (HAZ) which could be due to the heat retention from FZ. This zone width was varying from top to bottom with a decreasing width towards bottom. However, the coarsening effect is

different in different shielding condition and this may lead to difference in hardness values in that region. The microstructures of all the welds are free from both hot cracking and liquation cracking. With Helium gas as shielding, the fusion zone structure seems to be finer resulting in higher micro hardness value and the same discussed in 'hardness study' section. Compared to helium and argon, the sample prepared with no shielding gas shows more distinct fusion line and the fusion zone structure is comparable with argon gas shielding. Fig 4.11 shows the SEM photograph of fusion line of the weldments (3.0 kW laser power, 4 m/min speed and 18 l/min He flow rate) and compositional analysis on specific points within that obtained by EDS analysis are given in Table 4.2. Here it can be observed that there is no appreciable change in chemical composition which is essential for homogeneous mechanical properties. Similarly Fig. 4.12 and Table 4.3 represent information about fusion zone of the same weld. In FZ also the point to point compositional study shows homogeneity in the distribution. Comparing Fig. 4.11 and 4.12; Table 4.2 and 4.3 it can also be stated that from FZ to base material the elemental distribution has not been changed and at different points it is homogeneous.

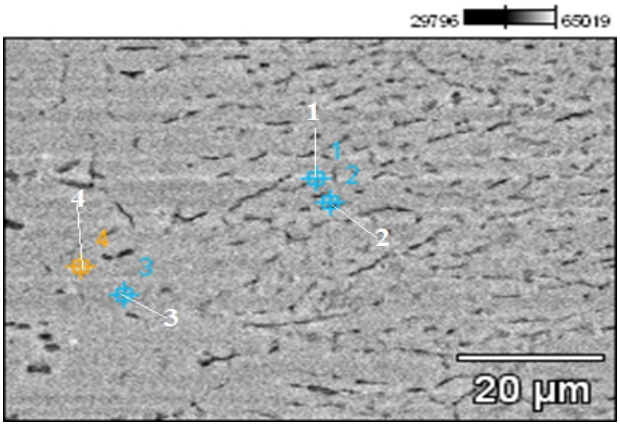

Fig. 4.11: SEM photograph of fusion line of the weldment

Table 4.2: EDS analysis based on Fig. 4.11

Position of study	**Composition (wt.%)**		
	Mg	**Al**	**Si**
Point 1	0.79	98.56	0.65
Point 2	0.59	98.63	0.78
Point 3	0.51	99.29	0.20
Point 4	0.92	98.69	0.38

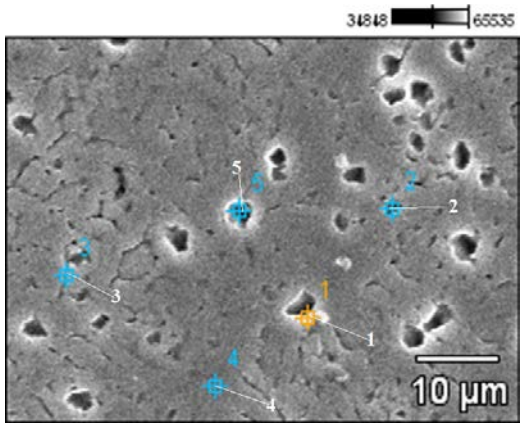

Fig. 4.12: SEM photograph of FZ of the weldment

Table 4.3: EDS analysis based on Fig. 4.12

Position of study	**Composition (wt.%)**		
	Mg	**Al**	**Si**
Point 1	1.03	98.12	0.84
Point 2	0.81	99.04	0.14
Point 3	0.77	98.71	0.51
Point 4	0.94	98.95	0.12
Point 5	0.95	99.00	0.05

4.3.3 Hardness study

Fig. 4.13 shows microhardness profile on cross sectional surface of laser welded aluminium alloy in as welded and in artificially aged conditions (aged for 2, 4 and 6 hour at 170º C). Base material hardness was found to be 115-120 $HV_{0.05}$ and in as welded condition a drop in hardness in fusion zone to a very low value (65 $HV_{0.05}$) was observed (Fig. 4.13a). Similar drop in HAZ was also observed. Moreover, the presence of HAZ is actually confirmed by the hardness test only. Comparing the macrograph, course grained region in micrograph and medium hardness values in the plot, the HAZ size can also be measured.

In general the lower hardness of FZ is due to the fact that the base material is in peak aged condition whereas fusion zone was in cast condition. The HAZ which is very narrow also shows low hardness as it may be in solutionized/annealed condition.

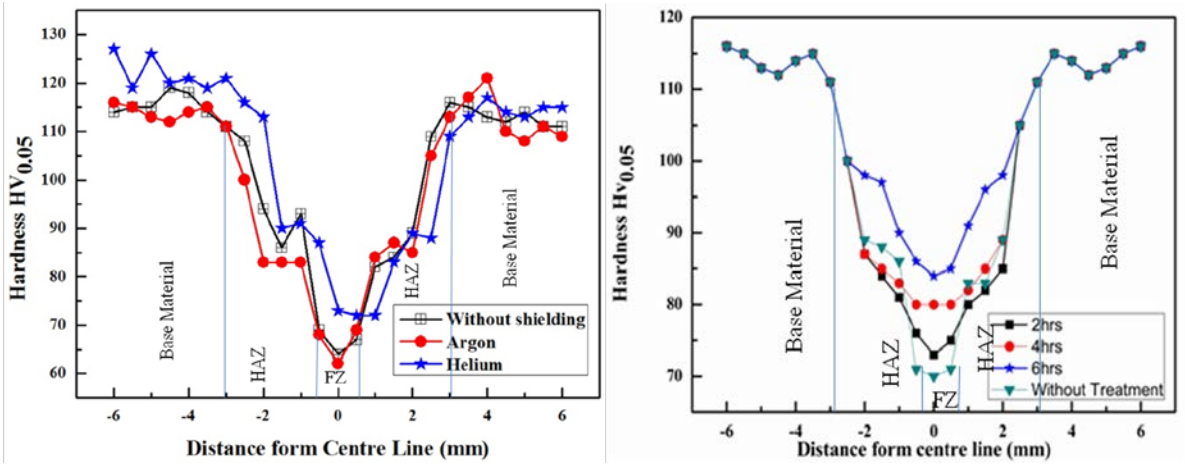

(a) (b)

Fig. 4.13: Microhardness profile on cross sectional surface of laser welded aluminium alloy in (a) as welded and (b) after post welding heat treated conditions (with Helium as shielding gas)

The difference in hardness data in the weld bead is due to microstructural variation, i.e. lower hardness was subjected to the coarse dendrite microstructure in fusion zone. The minor variation in hardness throughout the fusion zone would be due to the variation of dendritic arms spacing. The precipitation sequence of metastable phase in the 6061 alloy along the Mg_2Si pseudo binary line is as follows [55].

$$\alpha' \rightarrow \alpha + G.P \rightarrow \alpha + \beta'' \rightarrow \alpha + \beta' \rightarrow \alpha + \beta$$

The supersaturated solution α' is produced by solutionizing and quenching. The Gunnier-Preston (G.P) Zones are generated by the aging process below 170°C. The strengthening of 6061 alloy is ascribed to the precipitation of β'' in α-Al matrix during further aging. However, the β'' phase is stable only below 260 °C. During welding, the temperature at the heat-affected zone exceeds 260°C and causes over-aging of the alloy. This results in the coarsening of the β'' phase and the transformation of the β'' phase to the β' phase. The transformation of the β'' phase to the β' phase makes the alloy soften since the β' precipitates contribute less to hardening of the alloy than the β'' precipitates [56]. It may further lead to formation of α and β with more decrease in hardness values. If the cooling rate during the welding is sufficient to produce solutionizing effect again, then further aging may give rise to hardness parameter. In view of these, the butt welded specimens were subjected to artificial aging treatment to check any possible hardness recovery.

Fig. 4.13b shows that the hardness at the FZ was increased marginally by such treatment and the increase was more for higher holding time but the peak hardness even after 6 hrs was not

as per the base hardness. This may be attributed to the fact that the cooling rate during welding at FZ was not sufficient to hold the solutionizing affect fully and the heat treatment produces only minor amount of course second phase.

4.3.4 Tensile Testing

Tensile tests were conducted on base material and butt welded samples prepared with varying shielding gases, in as weld condition and post heat treated condition. Result of the same is tabulated in Table 4.4. It was observed that the welds have low tensile strength compared to the base material in general. This happened due to presence of cast structure in the FZ which subsequently did not undergo any precipitation hardening. The base material shows higher strength due to T6 treatment by which precipitation is obtained in the 6061 alloy along the Mg_2Si pseudo binary line. Moreover all the specimens have failed in the FZ due to its cast structure and the cracks were initiated at the fusion line, the weakest part of the weld. In case of yield strength also similar trend was observed.

Table 4.4: Tensile results of Base material and single pass welds with varying shielding gas condition at He-18l/min, 3 kW Power, 4 m/min Speed, Ar-22 l/min, 3 kW Power, 3.5 m/min Speed, without shielding-3 kW Power, 4.5 m/min Speed, Post weld Treatment (170^{o}C for 6 hrs)

Base material			Helium (As Welded)			Argon (As Welded)			Without shielding (As Welded)		
Yield strength (MPa)	Tensile strength (MPa)	Elongation (%)	Yield strength (MPa)	Tensile strength (MPa)	Elongation (%)	Yield strength (MPa)	Tensile strength (MPa)	Elongation (%)	Yield strength (MPa)	Tensile strength (MPa)	Elongation (%)
240±10	301±10	12	155±10	195±10	8	146±8	181±18	7	110±12	150±13	6.5
			Helium (Heat treated)			Argon (Heat treated)			Without shielding (Heat treated)		
			Yield strength (MPa)	Tensile strength (MPa)	Elongation (%)	Yield strength (MPa)	Tensile strength (MPa)	Elongation (%)	Yield strength (MPa)	Tensile strength (MPa)	Elongation (%)
			170±10	210±10	8	150±10	200±10	7	130±10	170±10	6.5

In case of welds with Helium as shielding gas marginal higher strength value was observed compared to the Argon and no shielding gas condition. The primary reason behind this may be the better penetration depth when Helium is used as shielding gas. Moreover, in case of no

gas condition there may be oxidation during the process and to ascertain that X-ray mapping of such weld was carried out with the EDS attachment of SEM. Fig. 4.14 shows such analysis and it revealed traces of oxygen in the weld. This may lead to formation of oxide inclusions, though such features could not be observed in the microstructure at the magnification level used here. Presence of such oxide helped in reducing the strength value of the weld in no gas condition.

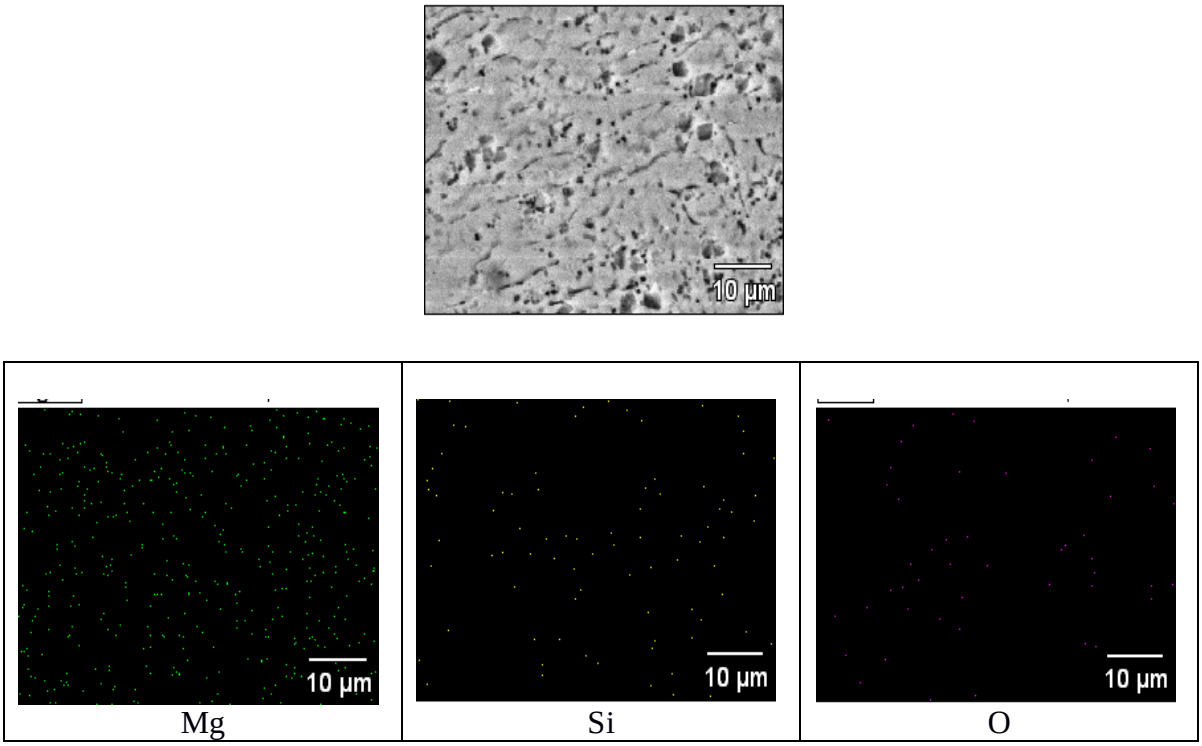

Fig. 4.14: Elemental mapping of FZ of weld with no shielding gas condition

From Table 4.4 it can be observed that even after post weld treatment there is not much improvement in strength of the welds compared to the values of base material. It may be due to non formation of super saturated solid solution in the weld structure which is the starting phase of such heat treatment. Analysis of the same is carried out in thermal modelling section.

4.3.5 Fractography

The fractured surfaces of the tensile samples were analysed under SEM and some fractographs are shown in Fig. 4.15. It can be observed that the fracture surface of the base

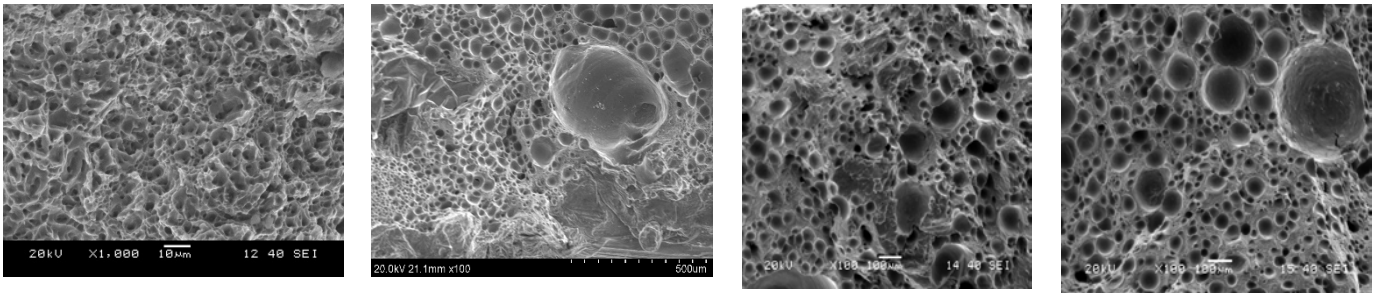

(a) **(b)** **(c)** **(d)**

Fig. 4.15: Fractured surface of (a) base material; welded with (b) Helium (c) Argon (d) No-Gas.

material represents ductile type of fracture due to presence of dimples. Moreover, it can also be observed that the dimples in base material are of similar size. In case of welded samples the basic appearance is similar, but they showed some larger dimple/void. This can be due to the presence of micro pores which was not detected earlier in micrographs. Thus apart from absence of age hardening phenomena, micro pores may have contributed to the lower strength value of the welded samples.

4.3.6 Formability Study

Erichsen Cupping Test was performed on base material sheet and the welded sheet to identify the change in ductility due to welding. Fig. 4.16 shows the result of the test performed on base material and single pass weld. It was observed that the I.E. value of the welded specimen is almost half of that of base material.

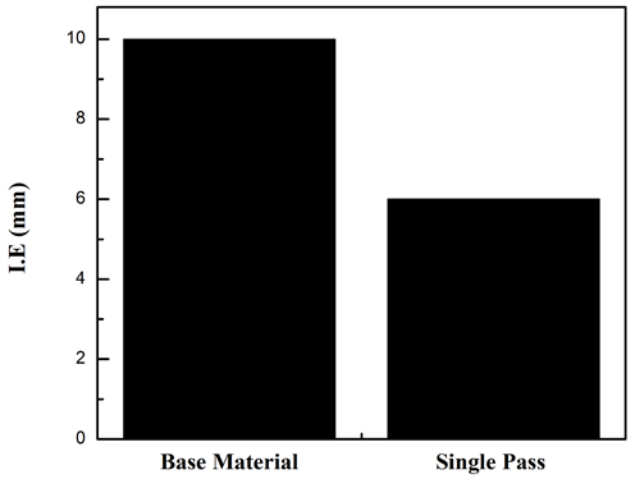

Fig. 4.16: Erichsen Index (I.E.) of base material and welded samples obtained by Erichsen Cupping test.

Fig. 4.17 shows the post formability test photographs of the samples. From this figure it can be observed that the weld has failed at the fusion line and base material shows more depth compared to single pass. The low formability of the welded sheet is attributed towards the fact the welded sample had brittle cast structure and it also contains micro porosity as observed in the fractograph. Moreover, formability can also be decreased due presence of thermal strain accumulated during the welding of the sheet.

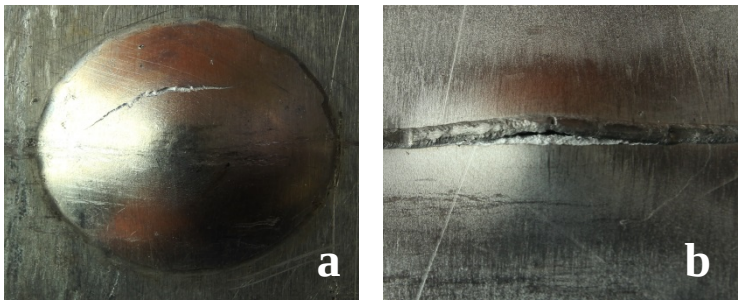

Fig. 4.17: Appearance of (a) base material and (b) single pass weld after Erichsen Cupping test.

4.3.7 Weld Thermal profile analysis

Modelling Of Thermal Profile

Temperature Profile

To figure out the microstructural changes after the welding in the weld zone, knowledge of the peak temperature and cooling rate that the particular zone has experienced is necessary.

Weld obtained by Helium as shielding gas was analysed by thermal equations as He produced best possible results in the current set of experiments.

Rosenthal equation [57], for a moving point heat source on a plate is given by

$$T - T_o = \frac{Aq/v}{2\pi\lambda t}\exp\left(-\frac{r^2}{4at}\right) \quad \text{..... 3.1}$$

Where T_0 is the Initial temperature of the substrate in (K),T is actual temperature at a position, where r is radial or lateral distance from weld, a is thermal diffusivity (64 m^2/s) [58], λ is thermal conductivity (167 $Wm^{-1}K^{-1}$)[58], q is heat input of the laser source (3 kW), v is welding speed (4 m/min), t is time elapsed from the state of movement of welding heat and A is absorptivity (0.12%) [59]. Fig. 4.18 shows distribution of such temperature T along with time t, at a particular distance r. It also shows plot at different r values i.e. temperature

profile of different points away from the centreline of the weld. Central line shows a peak temperature just above 1300 K and it drops rapidly with time.

Fig. 4.19 shows peak temperature distribution at different distance from central line towards the base material. This temperature vs. distance profile also confirms the fusion zone width or throat diameter as observed in Fig.4.6b plot. It depicts at approximately 1.0 mm of fusion zone around central line and is confirmed by low hardness values due to cast structure as shown in Fig. 4.13a/b.

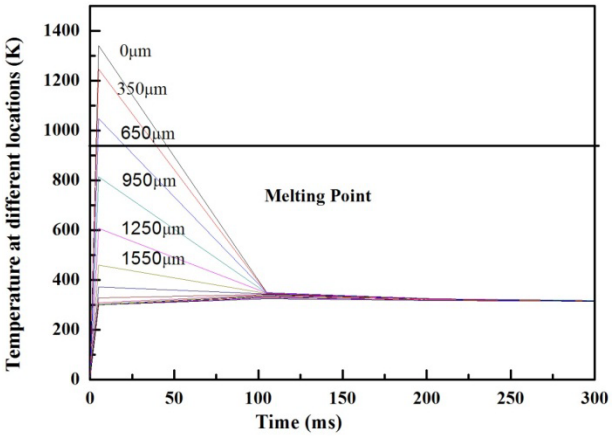

Fig. 4.18: Temperature distribution at different locations

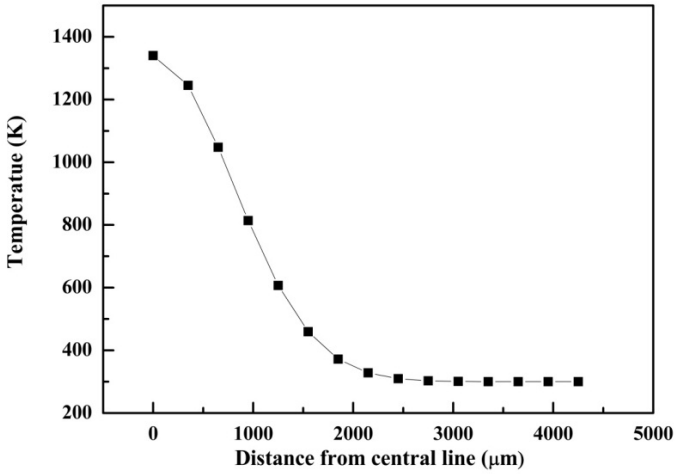

Fig. 4.19: Temperature distribution from centre line

Cooling Rates

Structure of a particular position in a weld zone (FZ and HAZ) depends upon the maximum temperature experienced at that position and associated cooling rate as the maximum temperature tells phase transformation and melting whereas cooling rate influences fineness of structure and formation of super saturated solid solution required for further aging treatment. To figure out these, cooling rate at a particular temperature was calculated by the following equation [57]

$$R = \frac{2\pi k\left(T_c - T_o\right)^2}{H_{net}} \quad \text{..... 3.2}$$

Where R is cooling rate at the weld centre line (K/s), λ is thermal conductivity of the material (167 $WM^{-1}K^{-1}$) [58]. $T_0$is initial plate temperature (K), $T_{c,}$ is temperature at which the cooling rate is calculated (K) and

$$H_{net} = \frac{power\left(p\right)}{speed\left(v\right)} \quad \text{..... 3.3}$$

Fig. 4.20 shows cooling rate vs. temperature profile for this particular butt welding experiment. It can be observed that in general cooling rate increases with temperature. Comparing Fig. 4.19 and 4.20 it can also be commented that maximum cooling rate decreases from central line towards base material. The maximum cooling rate of the Fusion Zone (at centre line) was approximately 17500 K/sec when the corresponding peak temperature is around 1300 K and minimum cooling rate of the FZ was approximately 7000 K/sec which corresponds melting temperature resulting in fine cast structure in fusion zone. But the cooling rate at lower temperature region wasn't enough to result in diffusion less cooling leading to super saturated solid solution in the weld structure [60]. That is why the hardness value was very low at the weld zone compared to the base metal even after post weld aging treatment as shown in Fig. 4.13b.

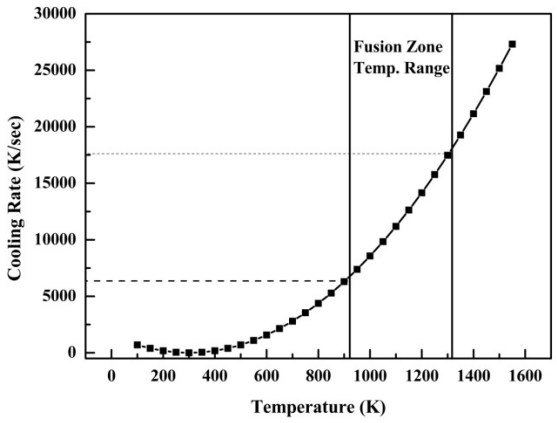

Fig. 4.20: Effect of cooling rate

4.4 Summary

The present chapter summarizes laser welding of 6061-T6 Al-alloy and subsequent characterization of the welds. Initially screening experiments were performed in Donut mode by varying welding parameters (Power, Speed and Shielding gas (He, Ar, without Gas)) to identify the parameters producing minimal defects. The optimised parameters

obtained from initial trials were used in actual butt welding experiment and the resulted welds were characterized by macro and microscopic observations, microhardness study, tensile testing and formability. The use of helium has produced better coupling compared to other shielding gas conditions. Hardness, strength and formability value of the welds were poor compared to the base material. After post weld treatment (aging cycle) the strength was increased marginally but base material strength could not be achieved. From the theoretical modelling analysis it was observed that the thermal profile experienced by the material during welding was insufficient to maintain T6 condition leading to loss of mechanical properties of the material. It was observed that optimized properties were obtained in butt joint produced by 3.0 kW laser power, 4 m/min speed and 18 l/min Helium flow rate.

Chapter 5: EFFECT OF LASER WELDING PARAMETER ON BEAD OVER BEAD WELDS

5.1 Introduction

In the earlier chapter it was observed that retention of the strength was not possible mainly due to the thermal condition and to improve the microstructure by refining, another laser pass with lower heat input was tried. The experimental challenge behind this was to focus the beam on the previous bead accurately and not to increase the bead width and thus Gaussian mode was tried for the second laser pass.

To finalise the second pass laser parameter in this mode, screening experiments was tried out first with bead on plate (BOP) experiments like earlier chapter. Experimenting over a wide range of laser parameters, successful process window obtained from BOP experiments was employed on actual butt welding experiments as Bead over Bead (BOB) Technique and resulting welds were characterized systematically. These second pass trial was carried out only on selected butt weld which showed best result as discussed in previous chapter. Thus, the butt weld produced with 3.0 kW laser power, 4 m/min speed and 18 l/min He gas flow rate in Donut mode was used as the starting material of the second pass experiment.

A DC035 slab CO_2 laser (Rofin-Sinar) fitted with 300 mm focal mirror which can yield spot sizes of 360 μm in Doughnut mode, and 180μm in Gaussian beam mode was used in this study. The laser parameters used in BOP was mentioned in experimental section in table 3.2 and were chosen systematically after analysing the results obtained from each set of parameters, sequentially.

The parameters screened from BOP experiments in terms of depth of penetration, weld width and minimal porosity and cracking were used for second pass welding experiments.

5.2 Effect of Welding Parameters in BOP Experiments

Fig. 5.1 shows the cross sectional macrostructures of some selected welds in terms of laser welding speed and laser power, in Gaussian mode. These macrostructure show the typical wine glass shape which is often found in laser welding. From the figure it can be observed that the Gaussian mode macrostructure has low bead width compared to donut mode

macrostructure as observed in earlier chapter. From the figure it can also be observed at 3 kW power and 4 m/min speed there is presence of liquation crack and this could be due to the differential contraction during cooling, inducing tension at outer edge i.e. fusion line and compression at its inner edge. The tensile condition at the outer edge is in the direction transverse to the weld and this is could be reason for cracking along the fusion line.

Laser Power (kW)	Welding Speed (m/min)			
	6	5	4	3.5
3	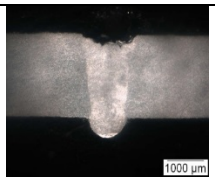	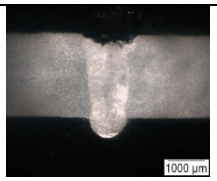	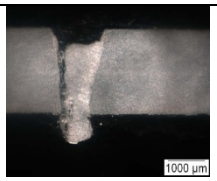	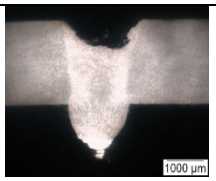
Laser Power (kW)	Welding Speed (m/min)			
	6	5	4	3.5
2.5	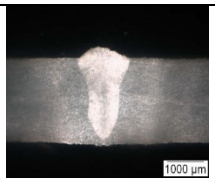	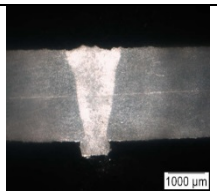	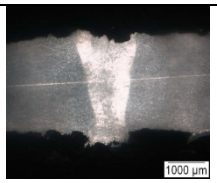	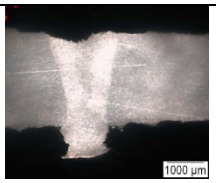
Laser Power (kW)	Welding Speed (m/min)			
	2			
2	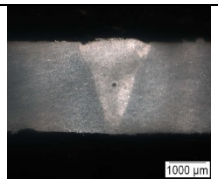			

Fig.5.1: Macrostructures of the BOP welds

From the figure it can be observed that at 2 kW power and welding speed of 2 m/min the shape of weldment is good but it contains porosity. This may be due to the reason that at lower speed keyhole stability is distributed as the vapour pressure in the keyhole is not sufficient to hold the thin molten metal layer lining.

5.3 Bead over Bead Laser Butt welding (Double pass)

The butt welding parameters were screened from BOP experiments in terms of penetration, weld width and minimal porosity and cracking. Butt welding parameters used for double pass weld are shown in table 5.1 and detailed analysis of the same is mentioned in subsequent

section. The characterisation results were compared with the previously obtained single pass weld (3.0 kW laser power, 4 m/min speed and 18 l/min He gas flow rate) to enumerate the changes obtained by the additional second pass.

Table 5.1: BOB Butt welding parameters.

Power(kW)	Speed(m/min)	Shielding gas (He) flow rate (l/min)	Pass
3.0	4	18	First pass
2.5	6	18	Second pass

5.3.1 Macrostructures

Fig. 5.2 shows macrostructure of single and double bead specimen; welded with parameters as mentioned in table 5.1. The macrostructures show that the welds are free from cracks. It can also be observed that fusion zone has a bright contrast compared to the base material and from this macrograph presence of Heat affected zone (HAZ) cannot be ascertained. In the macrograph of double pass welds two bright visible lines in the fusion zone were observed indicating the first and second laser scan weld pass.

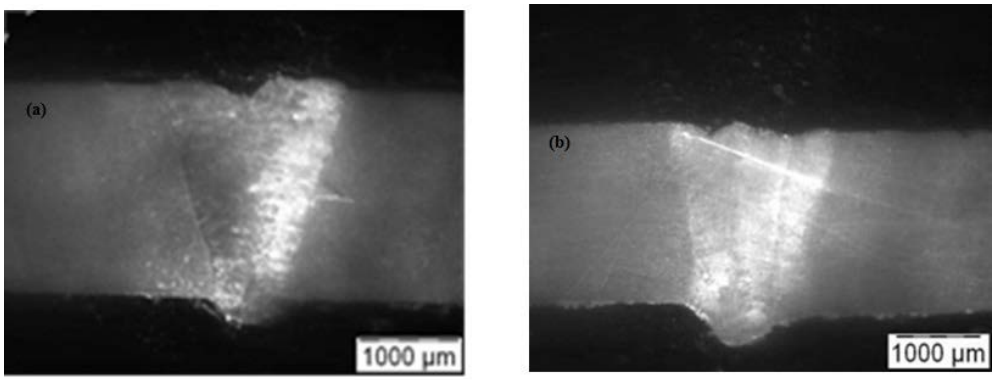

Fig. 5.2: Macrostructure of (a) single pass and (b) double pass

Fig. 5.3 shows the effect of welding pass on throat width and depth of penetration. Double pass welded samples showed marginally higher penetration depth and throat width compared to the single pass weld. Though the total heat input is more in case of double pass weld, the power input at a particular pass is not high compared to the single pass weld and the second pass/remelting may lead to refined structure.

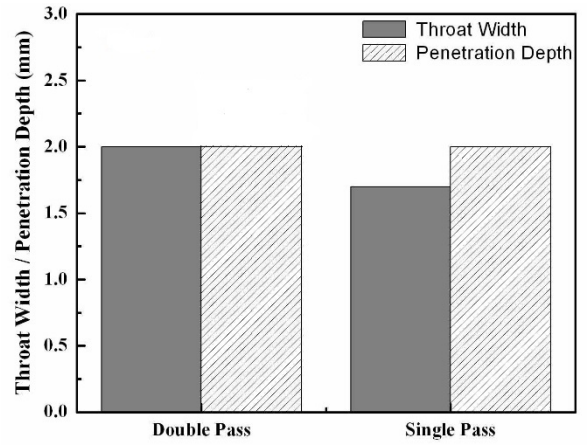

Fig. 5.3: Effect of welding condition on throat width and depth of penetration

5.3.2 XRD analysis

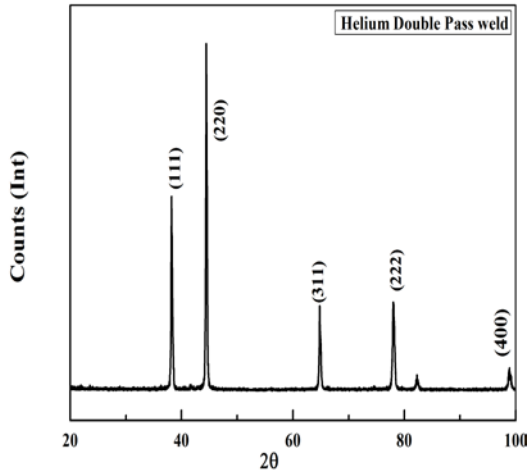

Fig. 5.4: XRD plot of Double Pass Weld

Fig. 5.4 shows the XRD profile of the double pass weld and it contains only α peaks similar to base material and single pass weld as shown in the previous chapter. Thus, from XRD, formation/change of phases due to the second pass could not be ascertained.

5.3.3 Microstructures

Fig. 5.5 shows optical micrographs of single and double pass welds (fusion zone and fusion line). In case of single bead weld it was observed that the microstructure of weld from base material to centre of the fusion zone was varying from cellular dendritic to columnar

dendritic and finally to narrow equiaxed dendritic. Variation in microstructure can result from different cooling rates and heat flow that could have resulted in different regions [61]. But, in case of the double bead welds, these distinguished regions were absent and this may be due to remelting of the existing first bead during second pass which was of lower heat input. Fig. 5.5(c) and 5.5(d) also indicate epitaxial growth near the fusion line which is a common phenomenon during welding. Adjacent to fusion line, towards the base material coarse grained structure heat affected zone (HAZ) was observed. In general the microstructures of the welds shown in Fig. 5.5 depict that the welds produced with single pass are having coarser structure compared to the double pass.

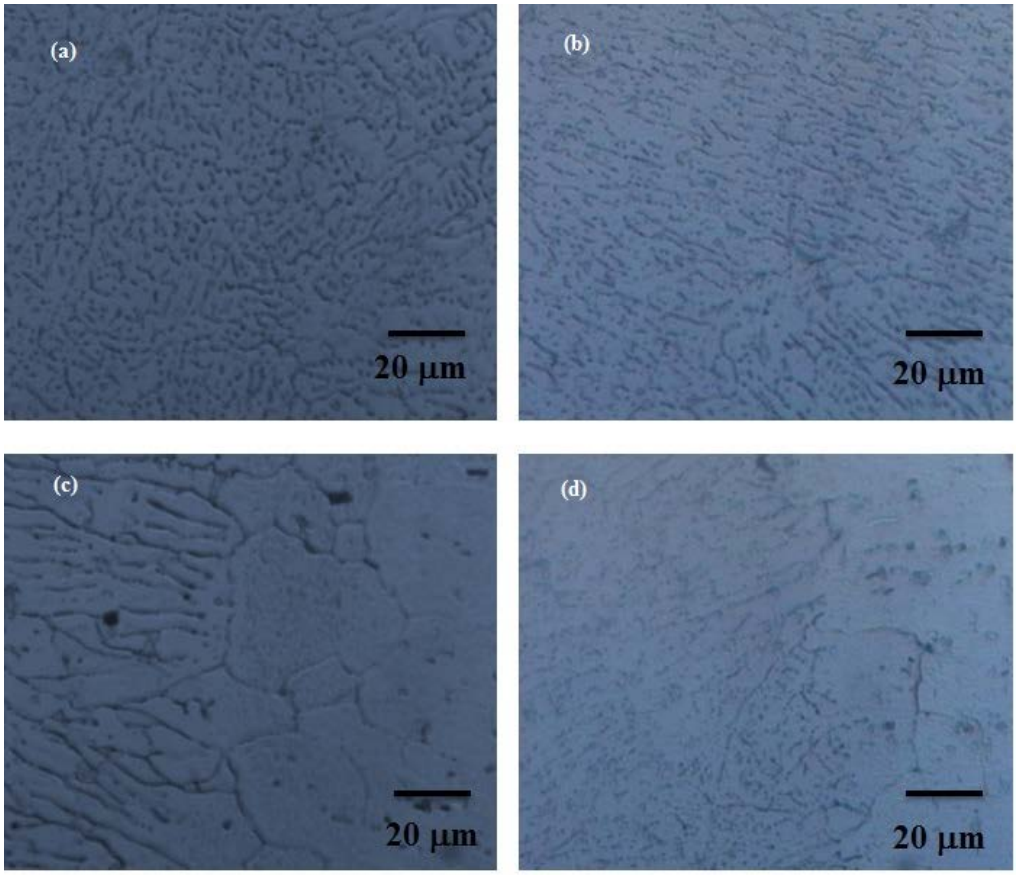

Fig. 5.5: Microstructures of (a) single pass FZ (b) Double pass FZ, (c) single pass fusion line and (d) double pass fusion line.

5.3.4 Micro Hardness Study

Figure 5.6 shows microhardness profile of single and double pass welds measured across the cross sections. Base material hardness was found to be 115-120 $HV_{0.05}$ and welds produced with single pass and double pass did not reveal much variation in their hardness trend. In both the conditions it was observed that fusion zone was having low hardness compared to the

base material. This is due to the reason that the base material is in peak aged condition whereas fusion zone (FZ) is in as cast condition. Marginal higher hardness in double pass specimen at the FZ may be due to the finer structure as shown in Fig. 5.5. After measuring the fusion zone from macro structure and comparing the same with micro hardness profile it can be ascertained that there exists a heat affected zone in between the FZ and the base material. The same was confirmed by the microstructural study (Fig. 5.5 (c and d)).

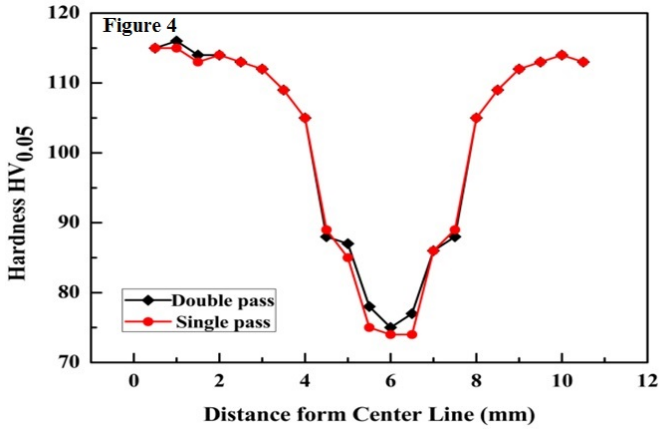

Fig. 5.6: Hardness profile of single pass and double pass welds (He gas)

5.3.5 Tensile Testing

Tensile tests were conducted on double bead welded samples and were compared with base material and single pass weld tensile data as obtained earlier. Those are tabulated in Table 5.2. The weld has low tensile strength compared to the base material basically due to presence of cast structure in the FZ which subsequently did not undergo any precipitation hardening. The base material shows higher strength due to T6 treatment by which precipitation is obtained in the 6061 alloy along the Mg_2Si pseudo binary line.

Table.5.2: Tensile results of single pass and double pass welds (He gas)

Base material			Single pass				Double pass			
Yield strength (MPa)	Tensile strength (MPa)	Elongation (%)	Yield strength (MPa)	Tensile strength (MPa)	Elongation (%)	Failure location	Yield strength (MPa)	Tensile strength (MPa)	Elongation (%)	Failure location
240±10	301±10	12	155±10	195±10	8	FZ	150±10	190±8	6	FZ

It was expected that tensile strength of the material would increase in double pass welding due to the refined cast structure but the experimental results showed decrease in tensile strength. This may be due to the additional micro porosities in the second pass welds as discussed in fractography section. Moreover, all the specimens have failed in the FZ due to its cast structure and the cracks were initiated at the fusion line, the weakest part of the weld. In case of yield strength also similar trend was observed.

5.3.6 Fractography

Figure 5.9 represents fractured surface of single pass weld and double pass weld obtained during tensile testing of the samples as mentioned in the previous section. It can be observed that the fracture surface appearances were basically alike for both the welds. Ductile type of fracture surface containing dimples can be observed both the fractographs. Apart from this feature, presence of micro pores were observed and number/size of such pores are little larger in double pass sample (Fig. 5.7b). This may have contributed to the marginal lower strength value of double pass weld.

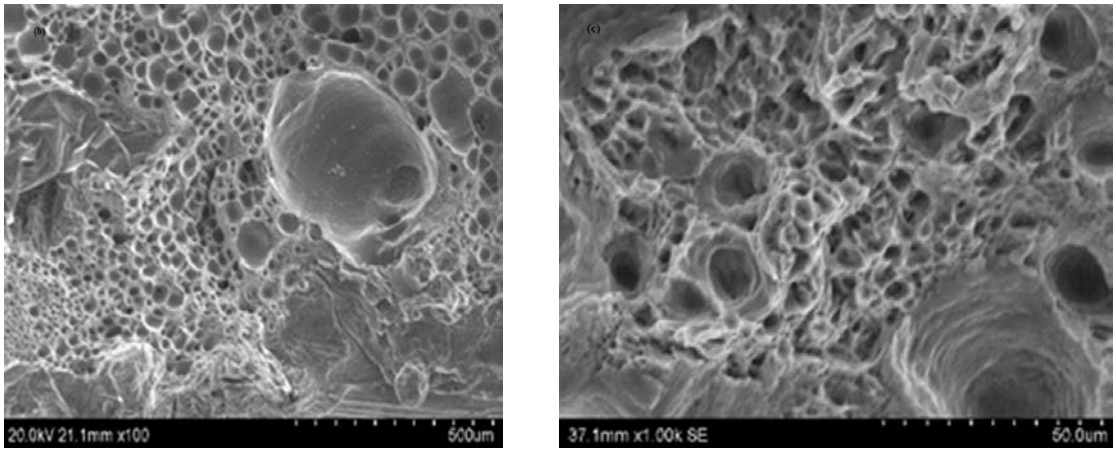

Fig. 5.7: Fractured surface of (a) single and (b) double pass welds.

5.3.7 Formability Study

Erichsen Cupping Test was performed to identify the change in ductility after performing double pass butt welding. Fig. 5.8 shows the result of the test performed on single pass weld and double pass weld.

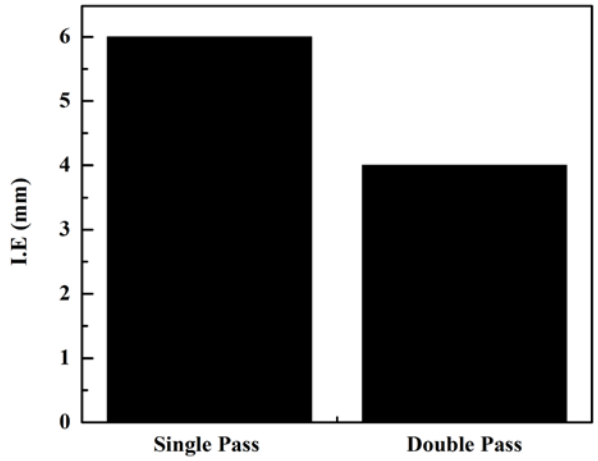

Fig. 5.8: Erichsen Index (I.E.) of single and double pass welded samples obtained by Erichsen Cupping test.

The figure shows that the I.E. value of the double pass welded specimen is lower than the pass weld. The reduction in formability in case of single and double pass welds can also be seen in Fig. 5.9 which shows the post formability test photographs of the samples. From Fig. 5.9 it can be observed that both the welds failed at the fusion line. This could be due to strain concentration occurring at the narrow and weak fusion line/HAZ and the strain accumulation. Lower formability value in case of double pass weld may also be due to the presence of more micro pores as mentioned in fractograph section.

Fig. 5.9: Appearance of (a) single pass (b) double pass welds after Erichsen Cupping test.

5.3.8 Fatigue Testing

Figure 5.10 shows high cycle fatigue test results of base material as well as single pass and double pass welded joints. The vertical axis shows the maximum stress (σ max) in MPa and the horizontal axis represents the number of cycles to facture. All the tests were carried out at room temperature with 15 Hz frequency with R (stress ratio) = 0.1. In general, both single

and double pass weld joints exhibited equivalent fatigue behaviour within the experimental scatter. When the stress amplitude was around 80% of yield strength (Y.S.), the weld joints showed marginal higher fatigue life compared to the base material tested at same percentage of stress amplitude. At 40% also similar trend was observed, but the weld's life is much better than the base material compared to the tests carried out at 80% level. It can also be observed that double pass welds showed marginally better fatigue life at 60% of its Y.S. compared to that of single pass welds.

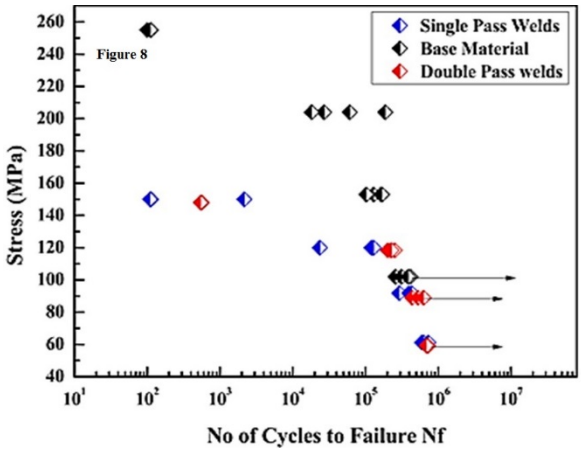

Fig. 5.10: Fatigue result of base material, single pass and double pass welds

Actually the fatigue resistance was susceptible to the presence of the soft material at FZ. This observation corresponds well to that reported by Roesler et al. [62] who pointed out that the fatigue strength of a material under dynamic cyclic loading was much more sensitive to the manufacturing process and material than the static strength, and the fatigue strength was also much more sensitive to the lower level of cyclic load than the higher level. In lower stress amplitude and longer life regime, the factors like surface conditions, residual stresses, localized stress concentration, surface protective coating, and severe weld concavity in weldments are deleterious to the fatigue life as reported by Anand et al. and Chowdhury et al. [63, 64]. In order to study variation in residual stresses, the welded joints and the base material were analysed by X-ray diffraction. Residual stress measurement by XRD showed base material stress at -318 MPa (compressive) and double pass welds at -19 MPa (compressive), whereas single pass welds showed 39MPa (tensile). This could be the reason that the double pass weld shows higher fatigue life compared to single pass welds at lower stress amplitude. But both of them show poor result compared to the base material due to presence of micro porosity and non aged condition.

5.3.9 Corrosion Test

Base material and welded specimens (single pass and double pass) were subjected to potentio-dynamic polarization test in a 3.6 wt. % NaCl solution to study the mechanism and rate of anodic dissolution. The polarization diagrams of all the specimens are shown in figure 5.11. Table 5.3 shows the summary of potentio-dynamic test results in terms of corrosion potential (E_{corr}), corrosion current density (I_{corr}) and corrosion rate. It can be observed that E_{corr} value is better in case of base material compared to both type of welds and in case of the welds there is no such variation. When the I_{corr} values were studied it was observed that corrosion current density is lowest in case of base material followed by the double pass weld. In case of corrosion rate opposite trend was observed it its value. Thus it is clear from figure 5.11 and table 5.3 that corrosion resistance of both single and double pass welds are less than the base material. But the double pass weld shows marginal better values compared to the single pass.

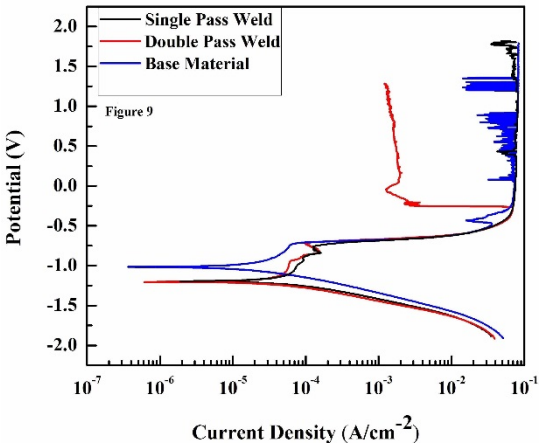

Fig. 5.11: Potentio-dynamic polarization behaviour of base material, single pass and double pass welds.

Table 5.3: Summary of potentio-dynamic test result

Sample	E_{corr} Observed (volts)	E_{corr} Calculated (volts)	Corrosion rate (mm/year) $x10^{-1}$	I_{corr}(A/cm^2) $x10^{-5}$
Base Material	-1.02	-1.01	5.16	4.67
Single Pass weld	-1.19	-1.19	10.01	9.25
Double Pass weld	-1.20	-1.20	9.94	9.10

Figure 5.12 shows post corrosion SEM photographs of all the specimens. There it can be observed that corrosion attack is severe in welded samples compared to base material. Presence of pits can also be observed in both single and double bead welds.

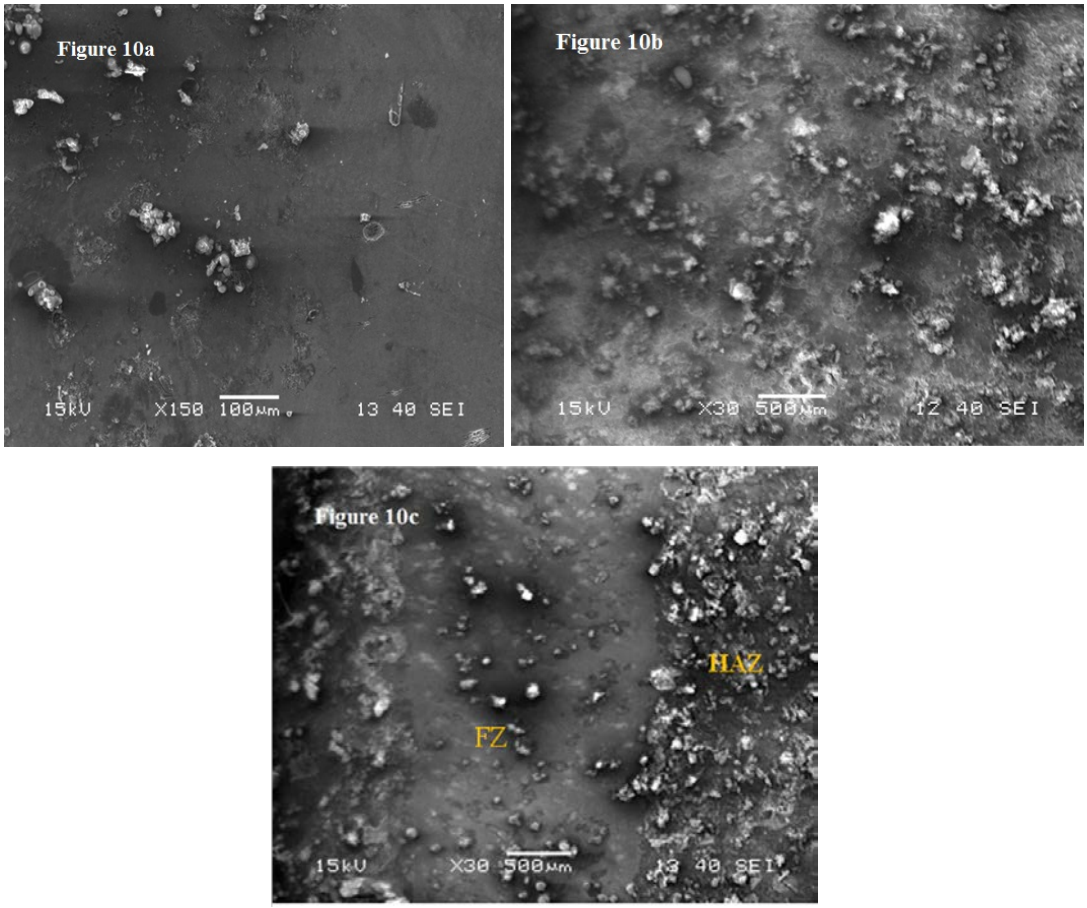

Fig.5.12: Post corrosion SEM micrograph of (a) base material (b) single pass and (c) double pass welds.

Earlier it was reported that due to formation of dendritic structure with heterogeneous concentration distribution the corrosion behaviour may be poor in welded samples [65]. In the current study presence of dendritic structure was confirmed in FZ (Fig. 5.5). Moreover, it was observed that single pass welds have tensile type of residual stress compared to the double pass, which could be a reason of marginal better corrosion behaviour of double pass weld.

5.4 Summary

The present chapter summarizes the effect of laser remelting/second pass lesser welding of 6061-T6 Al-alloy which was carried out to refine the microstructure and related change in mechanical properties. Initially screening experiments was tried out in Gaussian mode to

finalize second pass laser parameter (power, speed). He was selected as shielding gas for all the Gaussian experiments as it has shown better results compared to other shielding gases. For double pass butt welds combination of Donut + Gaussian mode was used sequentially with selected laser parameters obtained from trial experiments. After second pass, refinement of structure was observed but tensile strength did not show improvement. Some improvement in fatigue properties and corrosion behaviour was observed in double pass/remelted laser welds compared to single pass welds.

Chapter 6: CONCLUSION

From the present study the following conclusions can be drawn:

1. AA6061-T6 alloy samples were laser welded with single and double pass and the welds were free from visible defects such as cracks, under cut, over bead etc.
2. AA6061-T6 alloy laser welds produced with Helium as shielding gas has shown better characteristics due to its higher ionisation potential.
3. The hardness value was very low at the weld zone compared to the base metal even after post weld aging treatment but hardness of the FZ and HAZ of the specimen were increased after such heat treatment. After second pass/remelting there was marginal increase in hardness due to refinement in structure.
4. From the analytical modelling it was observed cooling rate was not enough to give super saturated solid solution in the weld structure. Due to this mechanical property of the welds is not at par with the base material.
5. Tensile strength values of both single and double pass welds were low compared to the base material due to their cast structure in the fusion zone and absence of precipitation hardening. The fractured surface showed ductile mode failure in all the specimens and micro pores in welded specimens.
6. Formability of the welds (single and double pass) was low compared to base material due to thermal strain concentration.
7. At lower stress amplitude double pass welds shows marginal higher fatigue life compared to the single pass welds possibly due to the finer microstructure in the fusion zone.
8. Corrosion resistance has decreased in both single and double pass welds due to cast structure. However, double pass welds showed slightly better corrosion resistance compared to the single pass welds due to its favorable stress condition.
9. In summary, some improvement in fatigue properties and corrosion behaviour was observed in double pass/remelted laser welds compared to single pass welds due to favourable residual stress level.

REFERENCE

1. Roy wood W. Development of aluminium alloys, Material and Design, 10, 8 (1989): pp. 248-253.
2. Penasa M, Rivela C. State of the art applications of aluminium alloy laser welding, Welding International, 21, 6 (2007): pp. 404-411.
3. Kudryashu O.N, Novikov O.M, Alekaserv I.V, Barabokhin N.S, Sabantsev A.N, Kapralov A, Kudryashov N.O, Ekoryavikhin. Welding aircraft structures from thick aluminium alloys, Welding International, 16, 5 (2002): pp. 412-414.
4. Sabe S, Eguchi N, Ema M, Matsumho T, Laser welding characteristic of aluminium alloys for automotive applications, Welding International, 17, 2 (2003): pp. 870-878.
5. Frolov V.A, Nikitina E.V, System analysis of the weldability of aluminium Alloys, Welding International, 22, 12 (2008): pp. 859-862.
6. Lakshminarayanan A.K, Balasubramanian V, Effect of welding processes on tensile properties of AA6061 Aluminium Alloy Joints, International Journal of Advance Manufacturing Technology, 40, (2009): pp. 286-269.
7. Hamada M, Control of Strength and Toughness at The Heat Affected Zone, welding international, 17, 4 (2003): pp. 265-270.
8. Bai Yan, Gao Hong Ming, Qui ling, Droplet Transition for Plasma-MIG Welding on Aluminium alloys, Journal of Translation of Nonferrous of Metal of China, (2010): pp. 2234-2238.
9. Dwivedi D.K, Influence of modifier and grain refiner on solidification behaviour and mechanical properties of cast Al-Si base alloys. IEI 83, (2002): pp. 46–50.
10. Kou S, Welding Metallurgy, Wiley Inter-Science, Canada, (2003): pp. 187–194.
11. Rao S.R.K, Madhusudhana G, Kamraj M, Rao K.P, Grain refinement through arc manipulation techniques in Al-Cu alloy GTA welds, Materials Science Engineering A 404 (2005): pp. 227–234.
12. Ellis M.B.D, Gittos M.F, Hadley I, Significance of liquation cracks in thick section welds in Al-Mg-Si alloy plate. TWI Journal 6, 2, (1997): pp. 213–255.
13. Yang Y.P, Dong P, Zhang J, Tian X, A Hot-Cracking mitigation technique for welding high-strength aluminium alloy, Welding Journal, 79, (1), (2000): pp. 10–14.
14. Manti R, Dwivedi D.K, and Agarwal A, Microstructure and Hardness of Al-Mg-Si

Weldments Produced by Pulse GTA Welding, International Journal of Advance Manufacturing Technology, (in press)

15. Cao X, Wallace W, Poon C, Immarigeon J.P. Research and progress in laser welding of wrought aluminium alloys I. laser welding process. Material Manufacturing Process, 18, 1, (2003): pp. 1-22.
16. Cao X, Wallace W, Immarigeon J.P, Poon C. Research and progress in laser welding of wrought aluminium alloys II metallurgical microstructures, defects and mechanical properties. Material Manufacturing Process, 18, 1, (2003): pp. 22-49.
17. Matrukanitz R.P, Selection and Weld-ability of heat-treatable aluminium alloys. ASM Handbook-Welding, Brazing and Soldering, 6 (1990): pp. 528–536.
18. William R, Oates, Editor American Welding society, welding hand book volume -3 Eight Edition Materials and Applications Part-1, 1996.
19. Ei-Batahgy A, Kutsuna M, Laser beam welding of AA5052, AA5083 and AA6061 aluminum alloys. Advanced Material Science Engineering 2009, ArticleId-974182, 9, doi:10.1155/2009/974182.
20. Matsunawa A, Katayama M, Kojima K, CO_2 laser weldability of aluminium alloys Report (I): Effect of Welding Conditions on Melting Characteristics. Welding International, 12, 7, (1998): pp. 519-528.
21. Padmanabham G, Shanmugarajan B, Experimental Investigation on Bead-on-Bead CO_2 Laser Welding of Al Alloy 6061, Proceedings of the 8th ASM Trends in Welding Research Conference, 22, 2008.
22. Dutta Majumdar J, Manna I, Laser Processing of Materials, Sadhana 28. (2003)
23. Steen W. Med, Laser material processing (springer). 1991.
24. Li Cui, Xiaoyan Li, Dingyaong He, Li Chen, Shuili Gong, Effect Of Nd:Yag Laser Welding on Microstructure And Hardness Of An Al-Li Based Alloy Materials Characterization 71 (2012): pp. 95-102.
25. Wu N.Q, Cedrixxia, Ming Li, Perrusquia Scott N, Mao X, Interfacial structure and micro and Nano mechanical behaviour of Laser Welded 6061 Aluminium Alloy Blank. Journal of Engineering Material Technology 126, 1, (2004): pp. 8-13.
26. Pastor M, Zhao H, Martukanitz R.P, DebRoy T, Porosity Under Fill and Magnesium Loss during Continuous Wave Nd: YAG Laser Welding Of Thin Plate of Aluminium Alloys 5182 and 5754. Welding Journal 78, 6, (1999): pp. 207-216.

27. John F Ready, Davo F Faraon. LIA Hand Book Of Laser Materials Processing, Publisher Laser Institute of America. ISBN 0912035153,158.
28. NarsimhaChary D, Ravi.N.Bathe, Basu A, Padmanabham G, Effect of shielding on autogenous laser welding of aluminum alloy 6061-T6, International Welding Symposium 2K12, 2012.
29. Bozzi S, A.L. Helbert-Etter T, Baudin A, Robineau J.C, Goussain, Mechanical Behaviour and Microstructure Of Aluminium-Steel Sheets Joined By FSSW, Texture, Stress and Microstructure, Article Id 36061. 2008.
30. Liu H.J, Fujii M, Maeda K, Nogi, Tensile Properties and Fracture Locations Of Friction Stir welded joints Of 2017-T351 Aluminum Alloy. Journal of Materials Processing Technology 142 (2003): pp. 692-696.
31. Higgins R.A, The Properties of Engineering Materials 2nd edition, Edward Arnold publishers, USA, 1994.
32. George E. Totten d, Scott Mackenzie, Handbook of Aluminium: Alloy production and Materials Manufacturing 1st edition, Marcel Dekker, inc, USA, 2003.
33. Liao J, Yamaoto N, Liu H, Nakata K, Microstructure at Friction Stir Lap Joint Interface of Pure Titanium and Steel. Materials letters, 64 (2010): pp. 2317-2320.
34. Madhusudhan Reddy G, Gokhale A.A, Prasad Rao K, Weld Microstructure Refinement In AA1441 Grade Aluminium-Lithium Alloy, Journal of Materials Science 32,(1997): pp. 4117-4120.
35. Gene Mathers, The Welding of Aluminium and Its Alloys 3rd edition, Wood Head Publishing, England, 2002.
36. Philips H,W.L, Equilibrium Diagram of Aluminium alloy systems. The aluminium Development Association, London, 196, pp. 128-133.
37. http://asm.matweb.com/search/SpecificMaterial.asp?bassnum=MA6061t6
38. Oosterkamp A.L, Djapic Oosterkamp, Nordeide A, Kissing Bond Phenomena in Solid State Welds of Aluminium Alloys, Welding Journal (2004): pp. 225-231.
39. Mondolfo L.F, Aluminium Alloys: Structure and Properties, Butter Worth's London 1976.
40. Hisashi Hori, Effect of Heat Affected Zone on Joint Strength Of Welded Al-Mg-Si System, Welding International 25, 10, (2011): pp.737-741.
41. Kutsuna M, Qu Yan, Study on Porosity Formation in Laser Welds in Aluminium Alloys (Report-2) Mechanical Porosity formation by hydrogen and magnetism, Welding International 13, 8, (1999): pp. 597-611.
42. Kutsuna M, Qu Yan, Study on Porosity Formation In Laser Weds In Aluminium Alloys

(Report-1): Effect of Hydrogen and alloying elements, Welding International 12, 12, (1998): pp. 937-949.

43. Greze A N, Morozenkov A.A, Efficiency of Laser Welding In Shielding Gases At A Higher density Of Radiation Power, Welding International 11, 7, (1997): pp. 548-550.
44. Utsumi A, Matsuda J, Yoneda M, Katsumura M, Effect of gas Flow Rate on Shape of Weld Bead Sections. Study on high speed surface treatment by arc with laser (2^{nd} report), Welding International, 15, 5, (2001): pp. 345-353.
45. Katayama S, Matsunawa A, Kojima K, Kuroda S, CO_2 laser Weldability Of Aluminium Alloys (Report 4) Effect of Welding Defects on Mechanical Properties, Deformation and Fracture of Laser Welds, Welding International 14,1, (2000): pp. 12-18
46. Katayama S, Solidification Phenomena of Weld Metals 2^{nd} Report Solidification Theory Solute Redistribution And Micro-Segregation Behaviour, Welding International, 14, 12, (2000): pp. 952-963.
47. Katayama Seiji, Mizutani Masami, Laser Weldability of Aluminium Alloys, Trans JWRI, 31,2, (2002): pp.147-155.
48. Akio Hirose, Hirotaka Todaka, Hiroto Yamaoka, Nobutaka Kurosawa, Kojiro F Kobayashi, Quantitative Evaluation of Softened Regions In Weld Heat Affected Zones of 6061 T6 Aluminum alloy Characterizing Of The Laser Beam Welding Process Metallurgical And Materials Transactions A, 30, (1999): pp. 2115-2120.
49. Mjujibur Rahman, A.B.M, Kumar, S, Gerson A.R, Galvanic Corrosion of Laser Weldment of AA6061 aluminium alloy, Corrosion Science, 49. (2007): pp. 4339-4351.
50. Yamoka H, Tsuchiya K, Hirose A, Kobayashi K, Study of Aging Treatment of Al Mg Si Alloy Laser Welds. CO_2 laser welding of Al-Mg-Si alloys 2^{nd} report welding international 15, 6, (2001): pp. 446-451.
51. Xie J, Kar A, Laser Welding Of Thing Sheet Steel With Surface Oxidation Welding Research Supplement, (1999): pp. 343s -348s.
52. http://en.wikipedia.org/wiki/Helium
53. http://hyperphysics.phy-astr.gsu.edu/hbase/tables/thrcn.html
54. Robert W, Messler Jr. Principles of welding processes, physics, chemistry and metallurgy, 2^{nd} ed, Wiley-VCH verlag GmbH and Co.KGaA, Weinheim (2004): pp. 65,163,175,.
55. Mondolfo, L. F. Aluminum alloys: structure and properties, 1st ed. Butterworth, London, (1976): pp. 644–651
56. Enjo T, Kurodo T, Microstructure in weld heat-affected zone of Al-Mg-Si alloy, Transaction Joining and Welding Research Institute.11, 1, (1982):pp. 61–66.

57. Brandes E.A, Brook G B. Smithells Metals Reference Book. 7 edition, British library Cataloguing In Publication Data.14-15.
58. John E Hatch. Properties and physical metallurgy, American society for metals, metals park.159. 1998.
59. Paleocrassas A.G, Tu J.F, Inherent instability investigation for low speed laser welding of aluminium using a single mode fibre laser. Journal of Material Processing, 210, (2010): pp. 1411-1418
60. Yue T.M, Yan L.J, Chan C.P, Dong C.F, Man H.C, Pang G.K.H, Excimer laser surface treatment of aluminium alloy AA7075 to improve corrosion resistance. Surface Coating. Technology, 179, (2004): pp.154-164.
61. Yang Z.B, Tao W, Li L.Q, Chen, Y.B, Li F.Z, Zhang Y.L, 2012. Double sided laser beam welded T joints for aluminium aircraft fuselage panels: process microstructure, and mechanical properties. Materials Design, 33, (2012): pp. 652-658.
62. Roesler J, Harders, H, Beaker,M, Mechanical Behaviour of Engineering Materials Metals, Ceramics, Polymers, and Composites 1sted.Newyork: Springer. 2007.
63. Anand D, Chen D.L, Bhole S.D, Andreychuck P, Boudreau G, Fatigue behaviour of tailor (laser) welded blanks for automotive applications. Material Science Engineering A, 420, (2006): pp. 199-207.
64. Chowdhury S.H, chen D.l, Bhole S.D, Powidajko E, Weckman D.C, Zhou Y, Fibre laser welded AZ31 Magnesium Alloy: Effect of welding speed on microstructure and mechanical properties, Metallurgical and Material Transaction A. 43 A (2012): pp. 2133-2147.
65. Xu Wl, Yue TM, Man H C, Nd:Yag Laser Surface Melting of Aluminium Alloy 6013 For Improving Pitting Corrosion Fatigue Resistance. Journal of Material Science. 43, (2008): pp. 948-951.

BIO-DATA

Name D.Narsimhachary
Date of Birth 28.07.1988
Permanent Address H.No15160, NBR (extn) Apartment,
NBR (extn) Colony, Meerpet,
Saroor Nagar Mandal,
Ranga Reddy District,
Hyderabad
500097
A.P.
E-mail ID vajraachary@gmail.com
Languages Known English, Hindi, Telugu

Educational Qualification

Examination	Discipline/ Specialization	School/college	Board of university	Year of passing	Class
B.Tech	Metallurgical and Materials Technology	MGIT, Hyderabad	JNTU, Hyderabad	2010	First class
Intermediate	Maths, Physics, chemistry	Sri Chaitanya Jr Kalasal, Hyderabad	Intermediate Board	2006	First class
SSC		Ravindra Shantiniketan High school, Hyderabad	SSC Board	2004	Distinction

PUBLICATIONS

Conference

- D. Narsimhachary, Ravi Bathe, G. Padmanabham, A. Basu, Effect of Shielding on Autogenous Laser Welding of Aluminium Alloy 6061-T6, paper presented at

International Welding Symposium 2K12 (IWS2k12), organized by BHEL Tiruchirappalli., in October 2012 held at Mumbai, India.

- D. Narsimhachary, Ravi Bathe, G. Padmanabham, A. Basu, Effect of Laser Wavelength on Laser Welding of Aluminum Alloy 6061-T6, NCPCM, organized by NIT Rourkela. December 2012 held at Rourkela, India.

Journal

- D. Narsimhachary, Ravi Bathe, G. Padmanabham, A. Basu, Influence of Temperature Profile during Laser Welding of Aluminium Alloy 6061 T6 on Microstructure and Mechanical properties, Materials and Manufacturing Processes DOI:10.1080/10426914.2013.872258.

- D. Narsimhachary, Ravi Bathe, G. Padmanabham, A. Basu, Microstructure and Mechanical Properties of Double Pass Laser Welds on Aluminium Alloy 6061 T6, Journal of Materials Engineering and Performance, (Submitted in Mar 2014).